Precambrian Research 411 (2024) 107525

Contents lists available at ScienceDirect

Precambrian Research

journal homepage: www.elsevier.com/locate/precamres

Chemostratigraphy of the Ediacaran Old Fort Point Formation in the southern Canadian Cordillera

Connor S. van Wieren *, Jon M. Husson, Blake Dyer

School of Earth and Ocean Sciences, University of Victoria, Victoria, British Columbia V8P5C2, Canada

ARTICLE INFO

Keywords:
Ediacaran
Old Fort Point Formation
Windermere supergroup
Diagenesis
Carbon isotope excursions
Shuram

ABSTRACT

The Ediacaran Old Fort Point Formation in the southern Canadian Cordillera records a large, highly negative carbon isotope excursion, with a minimum in the $\delta^{13}C$ values of marine carbonates of –12‰. Carbon isotope excursions are often interpreted to be broadly synchronous and to reflect shifts in the $\delta^{13}C$ value of marine dissolved inorganic carbon, possibly reflecting either fluctuations in the global proportion of organic matter burial, or post-depositional diagenesis. As diagenesis can create large discrepancies between the original $\delta^{13}C_{carb}$ value of the sediment and what is preserved today, it is essential to determine to what extent diagenesis has impacted these records. We measured carbon and oxygen isotopes on eight stratigraphic sections (n = 360), carbonate clasts from debris-flow deposits from the Old Fort Point Formation (n = 968), and major and trace elemental abundances (n = 249). We used these geochemical datasets to investigate whether local processes leverage a larger control on carbon and oxygen isotopic values rather than global processes. We argue that the carbonate strata with the lowest $\delta^{13}C_{carb}$ values (~ –12‰) are now calcitic but were neomorphosed from an aragonite precursor in a fluid-buffered, early diagenetic environment conducive to dolomite growth. Additionally, the recovery of the expressed excursion is preserved in carbonates that underwent early-marine diagenesis under more sediment-buffered conditions, with its geochemistry closer to the aragonite precursors. Tremendous variability, up to 17‰, is observed in $\delta^{13}C_{carb}$ values of clast populations from individual breccia horizons found in the in-fill of submarine paleocanyons, filled with material from underlying carbonates of the Temple Lake and Geikie Siding Members. The presence of such a large range of clast $\delta^{13}C_{carb}$ values requires an early acquisition of the observed Old Fort Point Formation $\delta^{13}C_{carb}$ values (pre-brecciation and submarine canyon incision) and precludes late-stage burial diagenesis. Moreover, despite disagreement with previously published geochronological constraints, we propose that the carbon isotope excursion recorded in the Old Fort Point Formation is equivalent to the widely studied Shuram excursion, the most negative carbon isotope excursion recorded in Earth history, and thus further geochronological work in the southern Canadian Cordillera is needed to test this proposition.

1. Introduction

The Ediacaran Period (~635–539 Ma; Knoll et al., 2006; Linnemann et al., 2019; Xiao and Narbonne, 2020) is an enigmatic period of both environmental and biologic changes to Earth's biogeochemical systems. Beginning in the wake of the Marinoan Snowball Earth glaciation (~639 – 635 Ma; Hoffman et al., 1998; Hoffmann et al., 2004; Condon et al., 2005; Prave et al., 2016), the Ediacaran also contains sedimentological evidence for the Gaskiers glacial period (~580 Ma, Pu et al., 2016). Sediments overlying Gaskiers diamictites contain fossil evidence for what is considered the initial radiation of large multicellular organisms assigned to the Avalon assemblage (e.g. Narbonne and Gehling, 2003; Xiao and Laflamme, 2009).

Following these changes to Earth's biosphere, measured values of the carbon isotopic composition of Ediacaran marine carbonates ($\delta^{13}C_{carb}$) are found to exhibit tremendous variability, with values ranging from + 8‰ to below –12‰ (Halverson et al., 2005). These large positive or negative deviations from long term average values of $\delta^{13}C_{carb}$ are referred to as carbon isotope excursions (CIEs). The largest of these excursions during the Neoproterozoic is known as the Shuram CIE (Burns and Matter, 1993; Fike et al., 2006; Husson et al., 2015), with nadir values of $\delta^{13}C_{carb}$ exceeding –12 to –15‰ (Busch et al., 2022).

* Corresponding author.
E-mail address: cvanwier@uvic.ca (C.S. van Wieren).

https://doi.org/10.1016/j.precamres.2024.107525
Received 6 February 2024; Received in revised form 27 May 2024; Accepted 18 July 2024
Available online 26 July 2024

Highly negative values of oceanic dissolved inorganic carbon (DIC) near –12‰ are impossible to explain using standard, steady-state carbon cycle models, as the input flux of carbon to the Earth's surface from the mantle is assumed to have a canonical $\delta^{13}C$ value of ~ –5‰ (Kump and Arthur, 1999), which is the minimum possible value for buried carbonate sediments in the absence of organic matter burial. The timing of this excursion has been constrained using Rhenium (Re) - Osmium (Os) geochronology in the Ediacaran between 574 ± 4.7 and 567.3 ± 3.0 Ma from organic-rich sedimentary deposits in north-western Canada and Oman (Rooney et al., 2020). Stratigraphically, the Shuram CIE occurs above the Avalon assemblage, postdating the origination of large eukaryotic organisms (Boag et al., 2024), but below beds containing some of Earth's first putative metazoans (560–549 Ma, Martin et al., 2000), the White Sea assemblage. Stratigraphically above the White Sea assemblage are fossils of the Nama assemblage, Earth's earliest putative biomineralizers (e.g. Wood and Curtis, 2015; Boag et al., 2016) occurring in the most terminal Ediacaran. It has been proposed that these radiations are broadly synchronous with increases in O_2 levels on Earth's surface (Fike et al., 2006; Sahoo et al., 2016), though some argue against this (Ostrander et al., 2023).

Stratigraphy with Shuram age-equivalent $\delta^{13}C_{carb}$ records have been observed on multiple paleocontinents including localities in South Australia (Husson et al., 2015), Oman (Fike et al., 2006), Death Valley, USA (Bergmann et al., 2011,), Peru (Chew et al., 2007, 2022), southern China (Jiang et al., 2007), and northwestern Canada (Macdonald et al., 2013; Moynihan et al., 2019; Busch et al., 2022; Busch et al., 2023). These strata share a number of characteristics. First, the excursion occurs stratigraphically above the ~635 Ma, post-Marinoan cap dolostones, and below beds containing the White Sea assemblage. Second, minimum $\delta^{13}C_{carb}$ values are ~ –12‰, which are followed by a gradual shift back towards ~0‰. Third, these records demonstrate low variability in $\delta^{13}C$ values between stratigraphically adjacent horizons of carbonate, and the isotopic excursion occurs over variable length scales (10's to 100's of meters) during a transgressive sequence. Finally, values of $\delta^{13}C_{carb}$ and $\delta^{18}O_{carb}$ at each locality are noted to covary (Grotzinger et al., 2011).

The causal mechanism of the Shuram excursion is contentious. There have been several models proposed to explain the generation of such negative $\delta^{13}C_{carb}$ values. Some models invoke the introduction of large quantities of isotopically light carbon to the Ediacaran ocean. Sources of light carbon can include remineralized methane (Bjerrum and Canfield, 2011) ($\delta^{13}C$ ~ –60‰), or large stores of remineralized organic matter with a $\delta^{13}C$ composition of approximately –26‰ (Rothman et al., 2003; Li et al., 2017). Alternatively, it has been proposed that diagenetic processes are responsible for the Shuram, where local processes, including recrystallization of primary carbonate minerals in the presence of isotopically light pore fluid, are the dominant drivers of the excursion (Bristow and Kennedy, 2008; Derry, 2010). It has also been argued that the Shuram excursion is unrelated to both changes in marine DIC, and local diagenesis. Rather, the Shuram has been inferred to be a record of locally enhanced evaporation and productivity related to global transgression in shallow carbonate platforms, geochemically disconnected from the marine DIC pool (Busch et al., 2022).

While Shuram equivalents have been identified previously in North America, no definitive observations have been made from the southern Canadian Rockies. Localities bearing strata with $\delta^{13}C$ signals interpreted to be Shuram-equivalents in North America include the Johnnie Formation of Death Valley, USA (Bergmann et al., 2011; Verdel et al., 2011) and the Gametrail and Last Chance Formations of northwestern Canada (Macdonald et al., 2013; Moynihan et al., 2019; Busch et al., 2022; Busch et al., 2023). In the southern Canadian Cordillera some samples from Ediacaran strata of the Old Fort Point Formation (OFP) within the Miette Group (Windermere Supergroup) are found to have extremely negative $\delta^{13}C_{carb}$ values as low as –12‰ (e.g. Smith, 2009; Lanni, 2017). Smith (2009) have attributed the highly negative values within the OFP to Marinoan post-glacial upwelling of isotopically light deep waters (originating from enhanced respiration of a large dissolved organic carbon reservoir at depth) into isotopically heavier shallow waters. Alternatively, on the basis of the magnitude of the $\delta^{13}C_{carb}$ values within the OFP, Lanni (2017) argued that this excursion must be correlative to the Shuram CIE. This study aims to further characterize the chemostratigraphy of the OFP in an understudied part of western Laurentia and provide both context and a potential mechanism for the generation of the highly negative $\delta^{13}C_{carb}$ values expressed in these carbonates within the southern Canadian Cordillera.

2. Geologic setting

The Windermere Supergroup (WSG), outcrops from northern Mexico to the Yukon, and consists of a ~3 to 9 km thick, Neoproterozoic to early Cambrian stratigraphic succession recording the breakup of the supercontinent Rodinia (Ross, 1991), and subsequent thermal relaxation and subsidence. The lowermost strata of the Windermere were deposited in fault-bounded basins interpreted to represent the rifting of Rodinia. These strata include mafic volcanics and glacial diamictite thought to be related to the Sturtian and Marinoan low-latitude glaciations (Rooney et al., 2015; Moynihan et al., 2019). Following rift sedimentation, thick successions of siliciclastics and rare carbonates are found during the transition from rifting to passive margin sedimentation along the western edges of Laurentia (Ross, 1991; Ross et al., 1995). The uppermost strata of the Windermere are truncated by the sub-Cambrian unconformity recognized across the Canadian Cordillera (Aitken, 1969; Ross, 1991). Strata of the Hamil Group above this unconformable surface mark the transition from syn-rift to post-rift deposits. However, this transition is noted to appear in younger sediments of the early to middle Cambrian in the Nadaleen River region of the Yukon (Moynihan et al., 2019) suggesting a diachronous end to rifting on the Laurentian margin. The strata of the Windermere in the southern Canadian Cordillera is predominantly silts, shales, and minor carbonates deposited in deep water through turbidity currents (Ross, 1991).

Like many Neoproterozoic successions, the Windermere Supergroup has sparse geochronological constraints. Maximum depositional ages (U-Pb on zircon) within Windermere basement rocks include a 740 ± 36 Ma age from the Mount Copeland gneiss in southwestern British Columbia (Parrish and Scammell, 1988), a 736 + 23/–17 Ma age from gneisses within the Malton Complex in southwestern British Columbia (McDonough and Parrish, 1991), and a 728 + 9/–7 Ma age from the Deserters Range Gneiss in northern British Columbia (Evenchick et al., 1984). A single zircon age of 569.6 ± 5.3 Ma from syn-rift intrusives of the Hamill Group (Colpron et al., 2002), which cross-cuts the Windermere and is evidence for an inferred second Neoproterozoic rifting event, constrains the earliest absolute age of the Windermere in the Canadian Cordillera. The minimum depositional age of the Windermere in the southern Canadian Cordillera is constrained by the presence of Early Cambrian ichnofossils (e.g. Gibb et al., 2017) within the McNaughton Formation of the Lower Cambrian Gog Group which unconformably overlies the Windermere (see Fritz and Mountjoy, 1975; Hofmann and Mountjoy, 2001).

In the southern Canadian Cordillera, between the Mount Robson area (British Columbia) and south of Lake Louise, Alberta, deposits within the middle Windermere are assigned to the Miette Group (Carey and Simony, 1985; McMechan and Waldron, 2015, Fig. 1). The Miette group is subdivided into three subunits: the lower, middle and upper Miette. The ~380 m lower Miette is dominantly comprised of calcareous sands, black slates and black limestone. The ~2870 m middle Miette, thickening westward, is dominated by interbedded sandstones, siltstones, pebbly grits, and rare limestones. The ~1800 m upper Miette is largely composed of slates and interbedded sands and siltstones (Carey and Simony, 1985).

Historically used as a marker unit within the Miette due to its

distinctly coloured siltstones, the Old Fort Point Formation (Smith et al., 2014) is a mixed carbonate-siliciclastic formation within the middle Miette Group that was deposited primarily during a transgressive sequence tract. This formation is comprised of three lithostratigraphic sub-units (members) which, in stratigraphic order, are the Temple Lake Member (TLM), the Geikie Siding Member (GSM), and the Whitehorn Mountain Member (WMM).

With an average thickness of 50 to 125 m, the TLM consists of purple-grey siltstones that transition into rhythmically bedded, cm- to dm-scale, turbiditic carbonates and siltstones that vary in colour from purple to green to red (Fig. 2A-C). Overlying the TLM, the Geikie Siding Member (~2 to 15 m) is comprised of grey-black mudstones and shales with elevated levels of total organic carbon (TOC - up to 4%, Smith, 2009) and authigenic carbonate nodules (Fig. S1) and carbonate-clast breccia horizons. It is from this unit that a single rhenium-osmium (Re-Os) isochron age of 607.8 ± 4.7 Ma (Kendall et al., 2004) was measured, and is currently the only estimate for the depositional age of the OFP. The transition from the rhythmically bedded carbonates of the TLM into the mudstones and shales of the GSM (which mark an inferred maximum flooding surface) suggests that the sequence represents base-level rise and cessation of carbonate deposition. The WMM (of variable thickness, < 0.5 to 165 m) is comprised of thick successions of conglomerates and breccias, with lithologically-diverse clast assemblages (Fig. 3), most of which are carbonate derived (including both limestones and dolostones). These clasts are interpreted to be eroded material from older OFP units and redeposited in this member, or else from a shallow-water carbonate platform that is either unexposed or not preserved. Localities where the TLM and GSM are completely removed and overlain by conglomeratic deposits that are several meters thick are interpreted to reflect the incision and infill of submarine paleocanyons (Smith et al., 2014) during base-level fall. Interbedded with the breccia horizons in the WMM, are several, ~1 m thick successions of dark, organic-rich carbonates representing the only observed carbonate sedimentation within the WMM other than transported carbonate clasts in debris flow deposits. Outcrops of the OFP in the Jasper region of the southern Cordillera are locally folded and faulted as part of the core of the Meadow Creek Anticlinorium (Charlesworth et al., 1967), indicative of the structural complexity of the region. Broadly, base-level is interpreted to rise throughout the deposition of the TLM until the GSM is deposited at maximum transgression. Additionally, there are two further base-level signals interpreted over the duration of WMM deposition: an initial base-level fall and associated mass-wasting and brecciation, and then a subsequent base-level rise as recorded by the return to carbonate deposition within the WMM (Smith et al., 2014).

3. Methods

3.1. Field methods

For all measured stratigraphic sections, carbonate samples were taken at ~0.1 to 1 m resolution (depending on the abundance of carbonate beds). Zones of high alteration such as veins, clear secondary mineralization, or extensively recrystallized beds, as well as beds with a high proportion of siliciclastic material relative to carbonate, were avoided when possible. In each section, when a debris flow deposit (such as a breccia or conglomerate) was encountered, between 10 and 100 carbonate clasts were sampled randomly across a 1 to 10 m along-strike distance (depending on thickness of the deposit) over the vertical thickness of the bed to produce a representative clast sample population. The lithology, facies, and colour of each sample was noted, as well as measurements of each clasts' long and short axis on the 2-D outcrop face. In siliciclastic-dominated localities where no in situ carbonate beds were present (OFP Landmark, Boomerang, Redoubt, Jasper - Highway 16), only breccias were sampled for carbonate clast populations as described above.

3.2. $\delta^{13}C_{carb}$ and $\delta^{18}O_{carb}$ analyses

Carbonate samples from both sections ($n = 360$) and clasts ($n = 968$) were slabbed perpendicular to bedding (when visible) to produce a fresh surface. Slabbed faces were visually inspected for zones of alteration such as veins, extensive recrystallization, fractures or weathered surfaces. Fine-grained material from visually unaltered zones were targeted and microdrilled using a carbide burr for approximately 10 to 100 mg of sample powders. Aliquots of these homogenized powders were used for all subsequent geochemical analyses. Approximately 2 mg of powder from each sample was weighed out and placed into individual borosilicate glass vials and heated to 90°C for ⩾12 h to remove remnant water. All samples were flushed with He, injected with 8 drops of 100% H_3PO_4 and allowed to react for ~ 45 min in a GasBox II preparation device at 85°C before being analyzed on a Sercon 20–22 continuous flow isotope ratio mass spectrometer (CF-IRMS) at the University of Victoria.

Replicate analyses of both primary standards (IAEA-603) and secondary standards (IAEA-CO8) as well as internal calcite standards (VTS, UVIC1, and UVIC3) were run bracketing natural samples to track the precision and accuracy of all measurements. Measurements of $\delta^{13}C$ and $\delta^{18}O$ were obtained simultaneously and data was corrected using the two-point scheme outlined in Paul et al. (2007). Measurement precision was assessed by population statistics on measured standards. Variability in IAEA-CO8 was 0.058‰ for $\delta^{13}C$ (1σ) and 0.197‰ for $\delta^{18}O$ (1σ) relative to the Vienna Pee Dee Belemnite (VPDB) standard. Variability of the VTS internal calcite standard measurements was 0.106‰ for $\delta^{13}C$ (1σ) and 0.213‰ for $\delta^{18}O$ (1σ).

3.3. Trace and major element abundances

Using aliquots of the carbonate powders prepared as described above, a subset of samples ($n = 249$) were prepared for trace and major elemental analysis. For each sample, 10 mg of powder was added to a 15 mL Falcon centrifuge tube, and a solution of anhydrous acetic acid (17.4 M), buffered with ammonium hydroxide (pH ~5) was introduced at a ratio of 1 mg: 1 mL (10 mL total). Each Falcon tube was rinsed once with 2% HNO_3, and three times with Millipore Milli-Q filtered water (18.2 MΩ) prior to use. Samples were then placed in a sonicator bath and allowed to react for 5 h before being centrifuged at 2500 rpm for 20 min. Following centrifugation, 1 mL of supernatant, clear of any insoluble residues, was extracted and pipetted into a second 15 mL Falcon centrifuge tube. To fix Ca concentrations in each tube to a target of 50 ppm, samples were further diluted with 7 mL of 2% HNO_3. The partial sample digestion method used here preferentially targets carbonate phases, leaving other phases (including siliciclastics) unleached. Thus, elements measured are assumed to be from carbonate-bound phases only.

Solutions were analyzed on an Agilent 8800–100 triple quadrupole inductively coupled mass spectrometer (ICP-MS) in single quadrupole mode at the University of Victoria for a suite of target elements. Internal standard elements In, Re, and Rh were analyzed in addition to target elements, and external calibration was conducted with a subset of serially diluted, multi-element sample solutions ($n = 4$) prepared using single element in–house stock solutions to approximate the concentrations of natural carbonate samples. Calibration curves using these external calibration standards were generated to calculate concentrations of unknown samples. To estimate precision, a drift solution was prepared from the mixture of a subset of diluted sample solutions reflecting the full range of observed carbonate sample lithologies (and inferred elemental ratios) and run bracketing natural samples. Measured percent error on drift solution replicates was 1.3% for Mn and 2.2% for Sr (1σ). Replicates of National Research Council of Canada (NRCC) reference material SLRS-5 were analyzed to further monitor precision and accuracy of natural samples. Replicate analyses of SLRS-5 yielded values of 4.16 ± 0.1 ppb (1σ) (accepted 1σ value of 4.33 ± 0.1 ppb) for

Mn, and 53.76 ± 0.6 ppb (1σ) (accepted 1σ value of 53.60 ± 0.7 ppb) for Sr. Elemental abundances are presented as molar ratios of each element X/(Ca + Mg) in either mmol/mol or μmol/mol (Ca + Mg). As the digestion method described above targets elements bound in carbonate phases only, normalizing each element to (Ca + Mg) allows for elemental interpretations to be made per mole of dissolved carbonate phase and for meaningful comparisons between limestones and dolostones.

4. Results

4.1. Lithostratigraphy

4.1.1. McBride Locality

At McKale Creek near the McBride, British Columbia region, a single section was measured through a succession dominated by coarse sands, carbonate-clast breccias, and dark limestone beds (see Fig. 4, panel 1, and associated inset a). Here, the first ~100 m of measured stratigraphy is characterized by sulfide-bearing, siltstones interbedded with sandstones. This siliciclastic unit is interpreted to be part of the Middle Kaza Group (Smith et al., 2014). Unconformably overlying these siliciclastics are mixed carbonate-siliciclastic breccias and conglomerates of the WMM with individual bed thicknesses of 0.8 to 2.0 m in thickness. Clasts of these breccias are comprised of a large range of lithofacies and sedimentary structures. These include individual clasts of dolostones and limestones of varying colours, displaying cross-bedding and wavy to planar laminations. Between these breccias are coarse-grained sandstones with abundant scours, channels and trough cross-bedding (e.g. Fig. 2E, F). Carbonate breccia units are overlain by siltstones before the first occurrence of in-place carbonate beds at ~165 m above the base of the section. Here, the carbonate beds display cross-bedding, are predominantly dark blue-grey and interbedded with beds more tan in colour suggesting an increased siliciclastic content (Fig. 2H-J). Carbonate beds continue uninterrupted until approximately 210 m above the base of the section where siliciclastics begin to dominate again. The top of the WMM here is covered.

4.1.2. Jasper localities

In the Jasper, Alberta region, the Old Fort Point Formation is much finer grained, and preserved carbonates reflect deposition via turbidity currents. In this region, four stratigraphic sections were measured, and two additional outcrops were sampled for carbonate-clast breccia populations. At the GSM Type localities (GSM Type 1–4, Fig. 4, panel 3), the lower ~100 m of measured stratigraphy in the TLM is comprised of purple-grey siltstones which grade into centimeter to decimeter-scale turbiditic carbonate-siltstone rhythmites (Fig. 2G). These rhythmic carbonates increase in frequency until the sediments become almost entirely carbonate. At this height, the carbonate rhythmites display stark shifts in colour from red to green and then back to red (Fig. 2A, B). Conformably overlying the TLM at this locality are dark, organic-rich siltstones of the GSM that grade into black mudstones over an interval of approximately 5 m. The GSM terminates with an ~2 m thick carbonate breccia of the WMM. Above these units, the succession is folded in a syncline and the measurement of further stratigraphy was not possible. Sections at Marmot Road and Pyrite Point both begin and end in rhythmically-bedded siltstones and carbonates and neither the base or top is exposed. Thus, these sections are interpreted to be entirely within the middle TLM. The total stratigraphic thickness of carbonate-bearing strata in this region is found to be < 40 m.

4.1.3. Lake Louise Localities

Stratigraphic sections of the OFP from Temple Lake and Wolverine in the Lake Louise, Alberta region are found to contain carbonate intervals that are much thicker than those in the Jasper region. In both stratigraphic sections, the stratigraphy largely matches that of the Jasper region, with purple-green siltstones of the TLM grading into colour-varying carbonate–siltstone rhythmites. However as mentioned, there is more carbonate in the Lake Louise region, with carbonate-rich intervals of up to 140 m (compared to ~40 m in the Jasper Region). Overlying the TLM at these localities, the GSM is exposed as grey-brown mudstones and is found to be overall coarser than the Jasper region. The GSM in this region is 5 to 7 m thick. Here, the WMM is interpreted to have been eroded completely, and the GSM is overlain by siliciclastics of the Middle Miette Group. A section was measured at the Railway locality in strata interpreted to underlie the Old Fort Point Formation, in the Corral Creek Formation of the Middle Miette Group. Here, the stratigraphy is dominantly siltstones that grade into carbonate-siltstone interbeds. Overall, all lithologies at Railway are much more siliciclastic rich when compared to those of the OFP. (see Table 1).

4.2. Chemostratigraphy

Carbonates of the Miette Group in the southern Canadian Cordillera consistently have a highly negative carbon isotope excursion. Across a northwest-southeast transect along the British Columbia-Alberta border (Fig. 1A), seven sections of the OFP (Fig. 4A-G) show a consistent excursion (in both magnitude and vertical stratigraphic expression) in all three of the geographic regions (McBride, Jasper, and Lake Louise; Figs. 1a-c, 2, 3, 4, panels 1, 3, 2). Beginning at the first occurrence of turbiditic carbonate beds in the lowermost TLM, values of $\delta^{13}C_{carb}$ are approximately –12‰, (varies from –11 to –13‰, Fig. 4). The downturn of the excursion is not preserved due to the lack of preserved carbonate in the lower TLM siltstones. Values of $\delta^{13}C_{carb}$ evolve from this nadir to approximately –7 to –8‰ by the uppermost TLM, at the base of the shales and mudstones of the GSM. This gradual transition from nadir values is found to accompany a lithological transition from dominantly silty carbonates into rhythmically bedded siltstones and eventually more pure carbonates.

Differences are observed in the thicknesses and variability in $\delta^{13}C_{carb}$ in the TLM between Jasper and Lake Louise. In the Jasper area, $\delta^{13}C_{carb}$ profiles display very little variability between stratigraphically adjacent samples, and the entire excursion spans between ~20 to 40 m of stratigraphy (Fig. 4, panels 3, 2, 6, 4). Conversely, in the Lake Louise area, while still relatively low, sample-to-sample variability is higher, and the excursion spans ~70 to 140 m of stratigraphy (Fig. 4, panels 10, 9). A measure of sample-to-sample variability was calculated by subtracting the data from a five-point running mean and the average offset is 0.18‰ in the Jasper area, and 0.44‰ in the Lake Louise area. Sections thicker than ~40 m (GSM Type, Temple Lake, Wolverine) show an inflection point in $\delta^{13}C_{carb}$ values. Here, values remain at or near minimum values (–12‰) for between 10 to 50 m of stratigraphy before beginning to rapidly increase towards –8‰ (Fig. 4).

Values of $\delta^{13}C_{carb}$ in the WMM at McKale Creek are generally more positive than at other localities, potentially due to basal erosion of carbonate with more negative $\delta^{13}C_{carb}$ values. Despite being exposed in

Table 1
Generalized field coordinates and labels for each locality as in Fig. 1 grouped by broad geographic region from north to south.

Region	Label	Locality	Latitude (°)	Longitude (°)
McBride, BC	1	McKale Creek	53.480723	–120.107131
Jasper, AB	2	GSM Type 4	52.872824	–118.287136
	3	GSM Type 1–3	52.872591	–118.291418
	4	Pyrite Point	52.861257	–118.064400
	4a	OFP Landmark	52.867671	–118.051455
	5	Jasper, Highway 16	52.860418	–118.185932
	6	Marmot Road	52.781676	–118.036099
Lake Louise, AB	7	Boomerang	51.471651	–116.142053
	8	Railway	51.459862	–116.267307
	9	Wolverine	51.435815	–116.080536
	9a	Redoubt	51.453381	–116.098483
	10	Temple Lake	51.366359	–116.168391

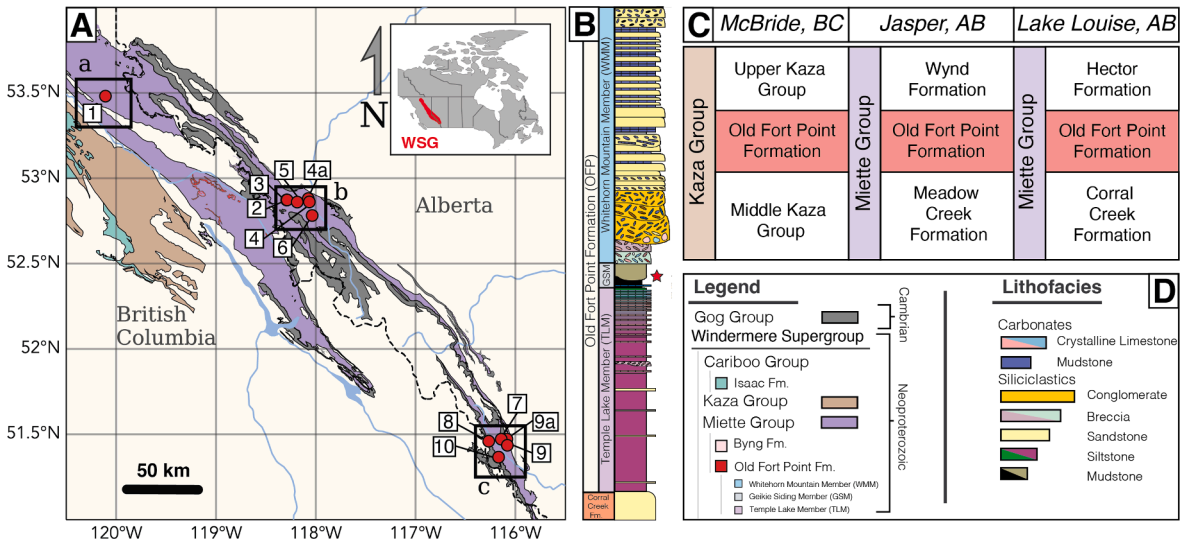

Fig. 1. (A) Map of the southern Canadian Rocky Mountains showing generalized field geology of the Windermere Supergroup (WSG) in the southern Canadian Cordillera with associated Groups and Formations and associated legend (D). Old Fort Point Formation localities are shown in the three broad regions (McBride, British Columbia; Jasper, Alberta; and Lake Louise, Alberta) with red markers. Numbered localities (1–10) are shown alongside each marker (Table 1). Generalized lithostratigraphy, modified from Smith et al. (2014) for the Old Fort Point Formation (relevant to localities in this study) is also shown in (B) with each member indicated. The red star indicates the stratigraphic location of samples analyzed by Kendall et al. (2004) for Re-Os geochronology. Regional formation equivalents and correlative formations for the three regions sampled in this study are shown in (C) following the correlation scheme presented in Smith et al. (2014). Note that the OFP appears both in the Miette and the Kaza Groups regionally as these two groups are approximately correlative. For more detailed maps of each region, see Fig. 4.

multiple localities (e.g. OFP Landmark, Wolverine, Boomerang, Redoubt, McKale Creek, GSM Type, Jasper - Highway 16), the WMM is only found to have in-place carbonate beds at McKale Creek in the McBride region (Fig. 4, panel 1). Here, underlying GSM and TLM are completely eroded (Smith et al., 2014), and the WMM overlies strata of the Middle Kaza Group (a regional equivalent to the Middle Miette Group, see correlations in Fig. 1C).

Values of $\delta^{13}C_{carb}$ in the WMM at McKale Creek are observed to be ~ –8‰ at the lowermost in-place carbonate bed and rise to near 0‰ by the uppermost carbonate bed over a thickness of approximately 100 m before the stratigraphy becomes dominated by siliciclastics. Further, sample-to-sample variability in $\delta^{13}C_{carb}$ values is considerably higher here (0.56‰ on average) than in Jasper or Lake Louise. A composite curve of $\delta^{13}C_{carb}$ and $\delta^{18}O_{carb}$ values for the whole Old Fort Point Formation is shown in Fig. 5A and B. In the Lake Louise region, a short section was measured in the silty carbonates of the Corral Creek Formation of the Miette Group (Fig. 4, panel 8) which underlies the TLM regionally (Smith et al., 2014). This section contains $\delta^{13}C_{carb}$ values that are constant over 10 m at ~ –10‰ suggesting $\delta^{13}C_{carb}$ values were very negative before deposition of the TLM.

Carbonates recording the Shuram excursion often show covariance between $\delta^{18}O_{carb}$ and $\delta^{13}C_{carb}$ values. Within the OFP, covariance is observed between carbon and oxygen at all localities. In the McBride area, the WMM at McKale Creek section has the most positive $\delta^{13}C_{carb}$ values, and has a Pearson r value of 0.18 (Fig. 5). In the Jasper regions, r values range from 0.13 to 0.70 with higher values found in thicker stratigraphic sections of the TLM. The Temple Lake section is found to have an r value of 0.33, but this lower correlation is driven by the inclusion of three outliers in $\delta^{18}O_{carb}$ (Fig. 5, Spearman's ρ has a value of 0.56). When values from all sections are combined, $\delta^{18}O_{carb}$ and $\delta^{13}C_{carb}$ have an r value of 0.58, a value that is higher on average than that of individual sections. Generally, the WMM displays the poorest $\delta^{18}O_{carb}$ - $\delta^{13}C_{carb}$ correlation ($r = 0.178$), and the TLM displays stronger correlation ($r = 0.13$ to 0.72, with an average of 0.47, Fig. 6).

4.3. Geochemistry of carbonate breccia clasts

Most breccia clast populations from the OFP have $\delta^{13}C_{carb}$ isotopic values spanning a range of several per mil, often encompassing the entire range of values found in the TLM stratigraphy. Distributions of $\delta^{13}C_{carb}$ values from clast populations of individual beds are shown in Fig. 7A-H. Sampled breccias broadly fall into two categories: breccias with largely homogeneous lithologic assemblages, often within the TLM (Fig. 3E, F), and heterolithic breccia assemblages including submarine canyon-fill material associated with the sea level changes during deposition of the WMM (Fig. 3A, C, D, G).

Breccias with homogeneous lithologic assemblage (Wolverine, Railway, Redoubt) have very little variability in $\delta^{13}C_{carb}$ values. Mean breccia bed thicknesses is 0.4 m and 0.7 m for Wolverine and Railway respectively. Observed changes in average $\delta^{13}C_{carb}$ value of individual breccia horizons at Wolverine track vertical shifts in the $\delta^{13}C_{carb}$ values of in-place section carbonates. At Railway and Redoubt, the range in $\delta^{13}C_{carb}$ is found to be –9 to –9.9‰ and –8.5 to –10.5‰ respectively (Fig. 7D, E), with clasts from Redoubt dominated by pink laminated limestones much like those comprising the TLM rhythmites. Clasts from OFP Landmark (minimum bed thickness of 18.5 m, as top and bottom contacts of the breccia unit were covered) are comprised almost entirely of pale pink-tan crinkle-laminated limestones and display a sizeable range of $\delta^{13}C_{carb}$ values of –10 to –13.5‰ (Fig. 7A).

However, despite showing little lithological diversity, samples from GSM Type, Jasper - Highway 16, and OFP Landmark all display a large range in clast $\delta^{13}C_{carb}$ values. At both GSM Type and Jasper - Highway 16, clasts from breccias are comprised almost entirely of carbonate mudstone clasts embedded in a sandy matrix (Fig. 3B), and display a variety of differing sedimentary structures including cross-bedding, and laminations. Values of $\delta^{13}C_{carb}$ from these beds have tremendous variability and range: –7.5 to + 1‰ and –7 to + 3.5‰ at GSM Type and Jasper - Highway 16 respectively. This range encompasses the entire range of TLM carbonates, but includes values from 0 to 3.5‰ that are not observed in TLM stratigraphy (samples more positive than the blue bar in Fig. 7G, H). Notably, clasts from OFP Landmark display fine, wrinkle-laminated fabrics that resemble those of cryptalgal microbialites.

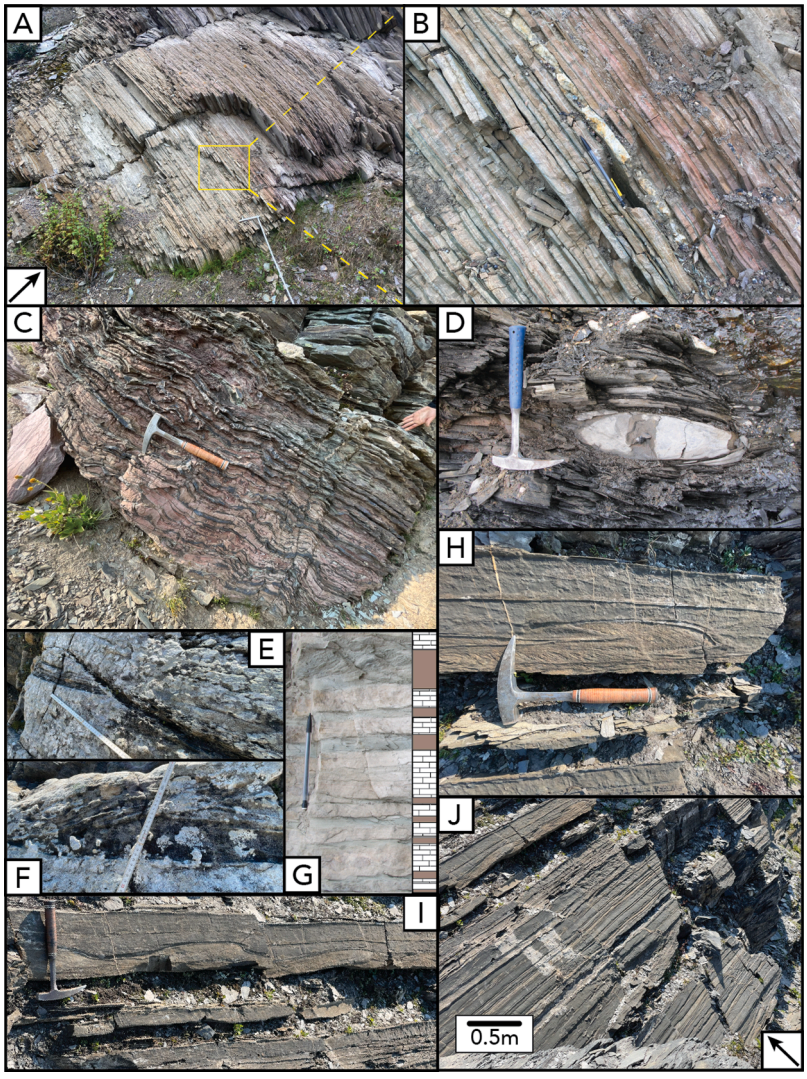

Fig. 2. Photographs of carbonate beds from Old Fort Point Formation stratigraphic sections (A-C), (G-J), and authigenic carbonates (D). Limestone-siltstone rhythmites of the upper TLM at GSM Type showing a green–red colour transition are shown in (A), (B), and (G). Dark, silty carbonates of the upper WMM at McKale Creek are shown in (H-J), with stratigraphic up indicated. (D) Authigenic carbonate nodules of the GSM at GSM Type. Sedimentary structures indicative of a higher-energy, shallower water environment are shown in (E), (F), (H), and (I). These include cross-bedding in coarse sandstones of the WMM (E, F), as well as scours in the sandy components interbedded with WMM carbonates (I), and convoluted bedding in (H).

Values of $\delta^{13}C_{carb}$ from breccia units with diverse, heterolithic assemblages are highly variable (ranges up to 16.9‰, Fig. 7F). Two localities reflect heterolithic breccia assemblages interpreted to reflect infill of submarine paleocanyons by collapse of canyon shoulder material (Smith et al., 2014): Boomerang and McKale Creek. Breccia beds of the Boomerang locality have a larger proportion of dolomite clasts, as well as a coarser, quartz-rich matrix (Fig. 3A). Mean breccia bed thicknesses here are 4.9 m, and values of $\delta^{13}C_{carb}$ range from –12 to –6.5‰ (Fig. 7C). At McKale Creek, mean bed thickness is found to be 1.5 m, and $\delta^{13}C_{carb}$ values show considerable variability within individual breccia horizons, with values from –13.5 to 3.7‰. The McKale breccias display values fully that fully encompass those of preserved OFP stratigraphy, as well as more positive values not preserved in the OFP strata (Fig. 7F). Notably, as shown in Fig. 6B, $\delta^{18}O_{carb}$ values are broadly most positive at Boomerang, and reach their most negative values at McKale Creek, with values approaching –24‰, while most OFP carbonates have $\delta^{18}O_{carb}$ values that range from –14 to –18‰.

4.4. Trace and major element abundances

Trace element ratios can be used to reconstruct the diagenetic history of marine carbonates. Of the nine elements chosen for elemental analyses, Sr/(Ca + Mg), Mn/(Ca + Mg), U/(Ca + Mg), and Mg/Ca are most useful in making such interpretations (e.g. Brand and Veizer, 1980; Higgins et al., 2018). Results for these select elements are summarized in Fig. 8, and a composite including Sr/(Ca + Mg), Mn/(Ca + Mg), and Mg/Ca ratios for the OFP is shown in Fig. 5. As shown by the data in red in Fig. 8A-B, A-B, samples from sections of the TLM (samples containing nadir $\delta^{13}C_{carb}$ values) show a generally negative correlation with both Sr/(Ca + Mg) and Mn/(Ca + Mg). Values range from 0.3 to 1 mmol/mol and from approximately 1.6 to 31 mmol/mol for Sr/(Ca + Mg) and Mn/(Ca + Mg) respectively. Within these ranges, $\delta^{13}C_{carb}$ values between –13‰ to –11‰ from the lower TLM are characterized by both high Sr/(Ca + Mg) and Mn/(Ca + Mg). Additionally, amongst nadir $\delta^{13}C_{carb}$ values at Temple Lake and GSM Type, some samples have elevated Mg/Ca ratios (up to 800 mmol/mol, Figs. 5, 8E), whereas most other samples have ratios < 50 mmol/mol. Throughout the recovery in $\delta^{13}C_{carb}$ values in the upper TLM, values of Sr/(Ca + Mg) and Mn/(Ca + Mg) decrease to

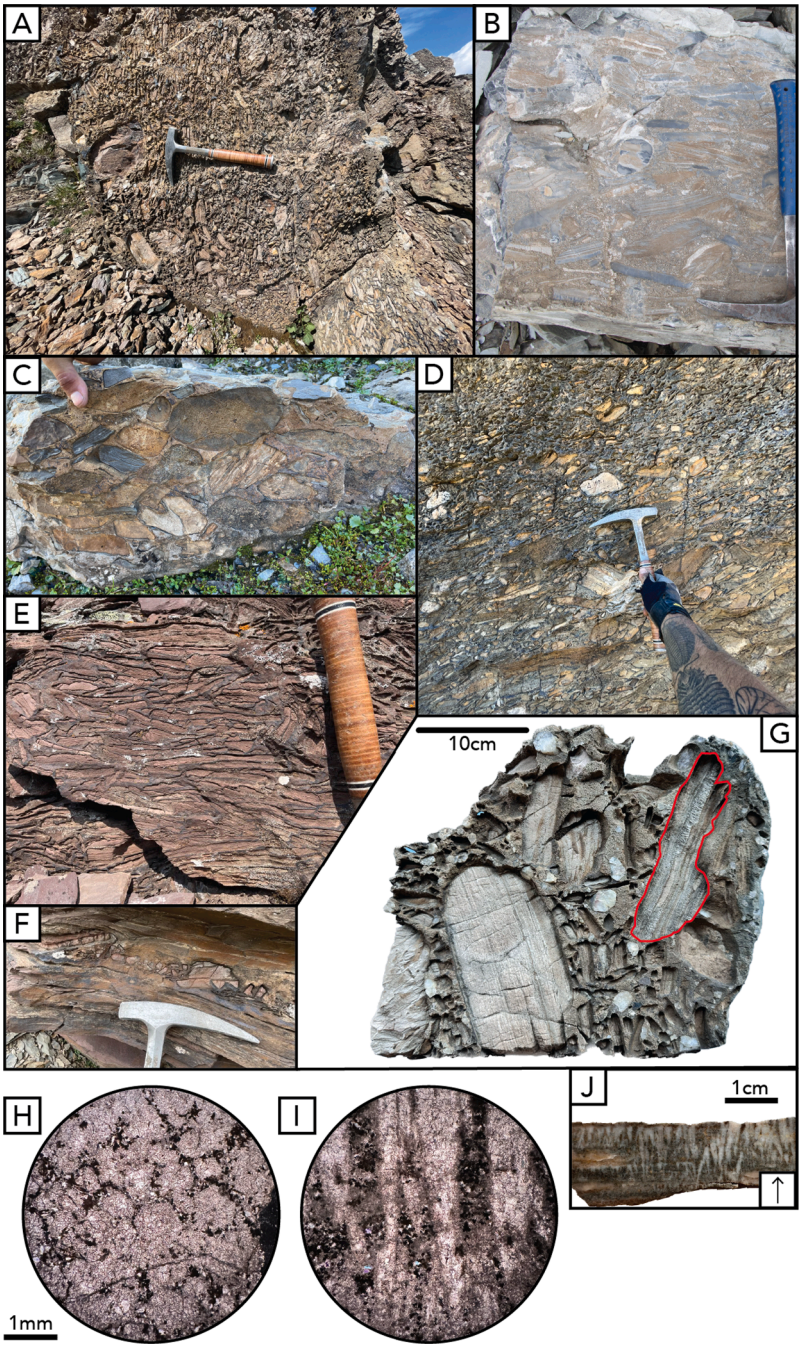

Fig. 3. Photographs of debris flow deposits of the Old Fort Point Formation. Canyon-fill breccias of the heterolithic clast assemblage are shown in (A), (C), (D), and (G). Intraclast breccias of the Temple Lake Member are highlighted in (E) and (F), and mudstone clast assemblage of GSM Type and Jasper - Highway 16 is shown in (B). A sample of a WMM breccia from Boomerang containing clasts of carbonate seafloor fans (highlighted in red) is shown in (G) and thin-section photomicrographs of this clast are shown in plan view (H) and cross-section view (I) demonstrating pseudo–hexagonal morphology. A polished sample of these fans in cross-section view is also shown in (J) with an arrow indicating stratigraphic up.

0.3 mmol/mol and 1.69 mmol/mol respectively (see also Fig. 5). Strata of the WMM at McKale Creek are characterized by much higher Sr/(Ca + Mg) than those of the lower TLM, and much lower Mn/(Ca + Mg). These ratios range from 0.75 to 5.69 mmol/mol and 0.31 to 6.71 mmol/mol for Sr/(Ca + Mg) and Mn/(Ca + Mg) respectively (Fig. 8A-B, A-B, Fig. 5), coinciding with an increase in coarse-grained siliciclastics, and a decrease in carbonate content. No clear relationship is observed between $\delta^{13}C_{carb}$ and either Sr/(Ca + Mg) or Mn/(Ca + Mg) within the WMM. Clast populations from GSM Type and Jasper - Highway 16 have positive correlations between Sr/(Ca + Mg) and $\delta^{13}C_{carb}$, with values of Sr/(Ca + Mg) ranging from 0.4 to 3.17 mmol/mol (something not observed in the stratigraphic data of the TLM). These clasts also show strong negative correlation with $\delta^{13}C_{carb}$ and Mn/(Ca + Mg). A similar negative correlation is also seen in TLM strata (Fig. 8B). In localities with breccias described as submarine canyon infill (Smith et al., 2014), clasts from McKale Creek have elevated Sr/(Ca + Mg) values of approximately 1.3 to 3.2 mmol/mol, and clasts from Boomerang are characterized by the lowest Sr/(Ca + Mg) values with most < 0.75 mmol/mol. Clasts from both McKale Creek and Boomerang are found to have Mn/(Ca + Mg) values from ~0.9 to 13.76 mmol/mol, much closer to the range in values that characterize the TLM. In these populations, Mn/(Ca + Mg) ratios

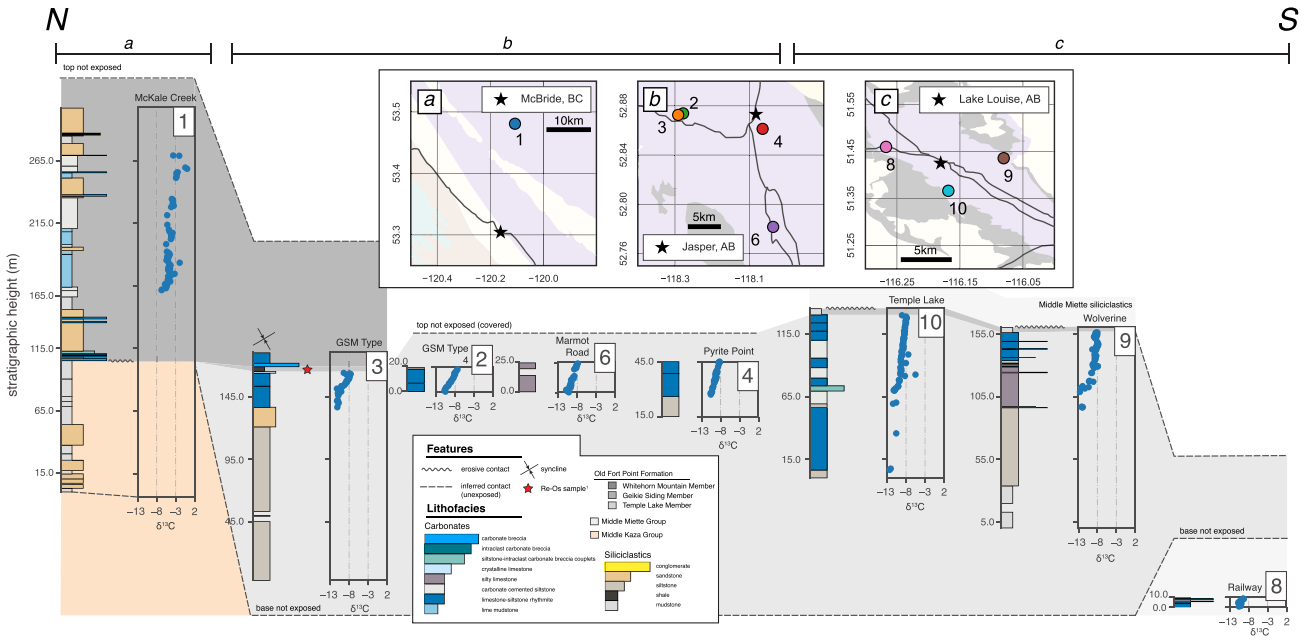

Fig. 4. Summary chemostratigraphy and lithostratigraphy for stratigraphic sections from the OFP with in-place carbonate beds. Sections are oriented broadly north to south by region (McBride, Jasper, and Lake Louise). All sections are aligned when possible on the inflection point from consistently nadir to more positive $\delta^{13}C_{carb}$ values. Scales on all y-axes are equal. Inset maps (a, b, and c) show each region with localities relevant to this figure identified as in Fig. 1. Major roads and cities are shown on each inset. For an explanation of section numbering and colours used for regional geology in the map insets, refer to Fig. 1 and Table 1.

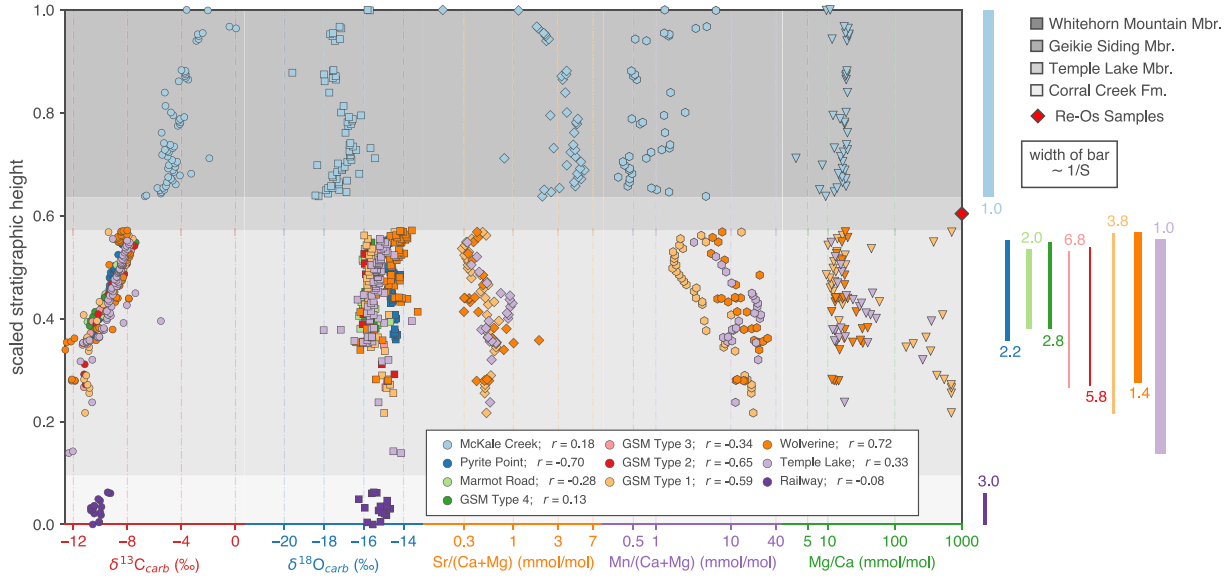

Fig. 5. Composite geochemical curves for the Old Fort Point Formation showing $\delta^{13}C_{carb}$, $\delta^{18}O_{carb}$, Sr/(Ca + Mg), Mn/(Ca + Mg), and Mg/Ca values and scaled stratigraphic height coloured by locality. Sr/(Ca + Mg), Mn/(Ca + Mg), and Mg/Ca are plotted and scaled logarithmically. Correlation coefficient (Pearson *r*) values between $\delta^{18}O_{carb}$ - $\delta^{13}C_{carb}$ values are listed for each locality. Sections were aligned and stretched based on their $\delta^{13}C_{carb}$ values, as well as the relative stratigraphic position of the TLM, GSM, and WMM members. Vertical height of boxes on the right (coloured by their respective locality) corresponds to the stratigraphic range for a given locality. The width of each bar correlates with 1/S where S is the scale factor used for each locality (each bar is also labeled with their scale factor). A red diamond indicates the stratigraphic position of the Re-Os age constraint from Kendall et al. (2004).

are largely < 10 mmol/mol, and values greater than this are predominantly from dolomitic clasts of Boomerang (with the exception of three clast samples from McKale Creek). Generally, $\delta^{13}C_{carb}$ values of all clast samples show a positive trend with Sr/(Ca + Mg) and a strong negative trend with Mn/(Ca + Mg). Irrespective of stratigraphic position, molar ratios of U/(Ca + Mg) have no observable trend with $\delta^{13}C_{carb}$, and most values are below 1 μmol/mol (Fig. 8D). However, samples from the TLM at GSM Type, Wolverine, as well as clasts from McKale Creek have elevated values closer to 4.5 μmol/mol. Clasts from breccias of McKale Creek have strong covariance between U/(Ca + Mg) and $\delta^{18}O_{carb}$, a trend not observed at any other locality (Fig. 8I). Mg/Ca ratios amongst clast populations have similar trends to the sections with values approaching 800 mmol/mol (Fig. 8I)

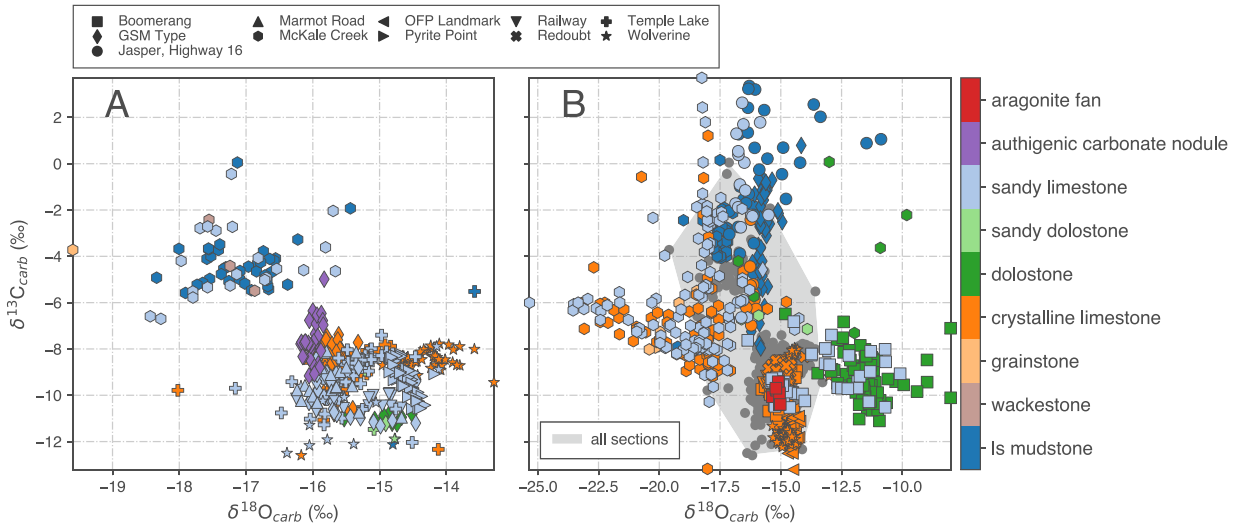

Fig. 6. Cross plots of $\delta^{18}O_{carb}$ vs $\delta^{13}C_{carb}$ coloured by sample lithofacies. (A) Data from all stratigraphic sections as well as authigenic nodules from the Geikie Siding Member (see 2D, Fig. S1). (B) Results from isotope conglomerate tests from clasts of the Old Fort Point Formation. Clast populations cover the entire range of $\delta^{13}C_{carb}$ and $\delta^{18}O_{carb}$ values found within underlying stratigraphy (shown in the region highlighted in grey) as well as populations of clasts displaying $\delta^{13}C_{carb}$ values more positive than preserved elsewhere in the OFP. Note, x-axis limits in (A) and (B) are not the same due to the large range in $\delta^{18}O_{carb}$ values expressed at McKale Creek.

5. Discussion

5.1. Geochemical trends – implications of isotope conglomerate tests

Sections of the Temple Lake Member at all localities demonstrate a consistent excursion in $\delta^{13}C_{carb}$ values interpreted to be a basin-wide signal. The basal TLM is characterized by $\delta^{13}C_{carb}$ values of –12‰ that evolve to ~ –7 to –8‰ at the base of the WMM. Values continue to rise throughout the WMM to ~0‰. The regional similarity in the stratigraphic expression of this excursion seems to preclude an interpretation of entirely local processes controlling the isotopic trends in the OFP, however, the highly negative values observed are difficult to reconcile with simple models of the carbon cycle. It is possible to generate regional trends in $\delta^{13}C_{carb}$ during early diagenesis and thus, we must consider the impact of such processes on the OFP.

Using $\delta^{13}C_{carb}$ and $\delta^{18}O_{carb}$ values from clasts derived from conglomerates and breccias of the Old Fort Point Formation, isotope conglomerate tests (e.g. Husson et al., 2012) were performed to constrain the relative timing of acquisition of the OFP $\delta^{13}C_{carb}$ excursion, specifically targeting the thick, canyon-fill breccias of the WMM. These deposits are useful as they represent large erosive events that we infer to re-mobilize significant portions of underlying stratigraphy. As demonstrated by Smith et al. (2014), localities such as Boomerang, McKale Creek, and OFP Landmark with erosive bases and complete removal of the underlying TLM and GSM have been interpreted as such paleocanyon-fill breccia successions. If carbonate beds are successively deposited in a basin that reflects the isotopic composition of seawater, which is evolving with time, and these beds were eroded and re-mobilized, the resulting breccia should contain clasts that have the full range of $\delta^{13}C_{carb}$ values observed in the originally eroded beds. If clasts within this breccia were reset isotopically during diagenesis after deposition, the isotopic variance within the clast populations should be proportional to the extent of diagenesis. In this case, increasing interaction with diagenetic fluid will yield increasing isotopic homogeneity in clast populations. Thus, if clasts in a sampled breccia within a section were found to display the same range as the intact stratigraphy, we would conclude that the geochemical composition of the breccia (and through inference, the section containing the breccia) was acquired early – i.e., before the brecciation event.

Clast populations across the OFP generally show a significant range in $\delta^{13}C_{carb}$ values of up to 17‰ (Fig. 7). These large ranges in $\delta^{13}C_{carb}$ values are primarily from breccias with heterolithic clast assemblages, however as mentioned previously, localities with clast populations with more homogeneous lithologic compositions such as OFP Landmark, Redoubt, GSM Type, and Jasper - Highway 16, display $\delta^{13}C_{carb}$ ranges of up to 10‰. Localities that display little variance in individual beds (e.g. Railway, Wolverine) are interpreted to be intraclastic breccias representing small-scale erosive events only mobilizing a few beds of underlying stratigraphy. This is corroborated by the colour, lithology, as well as relationship to underlying stratigraphy (see Fig. 3E-F). The observed range in $\delta^{13}C_{carb}$ values in clasts cover the entire range of underlying WMM and TLM stratigraphy, suggesting that the dominant source of these breccias is material from these units themselves. As shown in Figs. 6B, and 7, there are a number of samples with $\delta^{13}C_{carb}$ values more positive than those preserved in the Old Fort Point Formation and hence must have been sourced from carbonate sources either unpreserved, or eroded out during WMM deposition. If the $\delta^{13}C_{carb}$ signal recorded in the Old Fort Point Formation was purely the result of a late-stage diagenetic process (i.e. burial diagenesis) we would expect the distribution of $\delta^{13}C_{carb}$ values across clast populations to be more homogeneous.

The extreme variability in clast populations within each individual breccia horizon (a "pass" of the isotope conglomerate tests) suggests an early, pre-brecciation acquisition of the OFP $\delta^{13}C_{carb}$ signal. In other words, $\delta^{13}C_{carb}$ values of carbonates in the OFP (both within breccias, and by extension, in the sections) could have been acquired post- or syn-depositionally, but pre-brecciation and submarine canyon incision. This does not preclude a diagenetic origin, but makes late-stage (e.g. burial) diagenesis extremely unlikely. There are two possible interpretations for this result: *(1)* the $\delta^{13}C_{carb}$ values obtained by the OFP are reflective of Ediacaran seawater DIC (i.e. a primary origin); and *(2)* the OFP $\delta^{13}C_{carb}$ values reflect extremely early-stage diagenesis that took place shortly after deposition, but before the beds were remobilized as breccias.

5.1.1. Geochemistry of seafloor precipitates

Clasts from canyon-fill breccias of the WMM at Boomerang reveal fan-like carbonate crystal structures as described previously (Fig. 3G-J). Photomicrographs of these fan-like crystal structures (Fig. 3H, I) display clear pseudo–hexagonal structure, indicative of an aragonitic precursor (Bragg, 1924) despite having been neomorphosed to a current

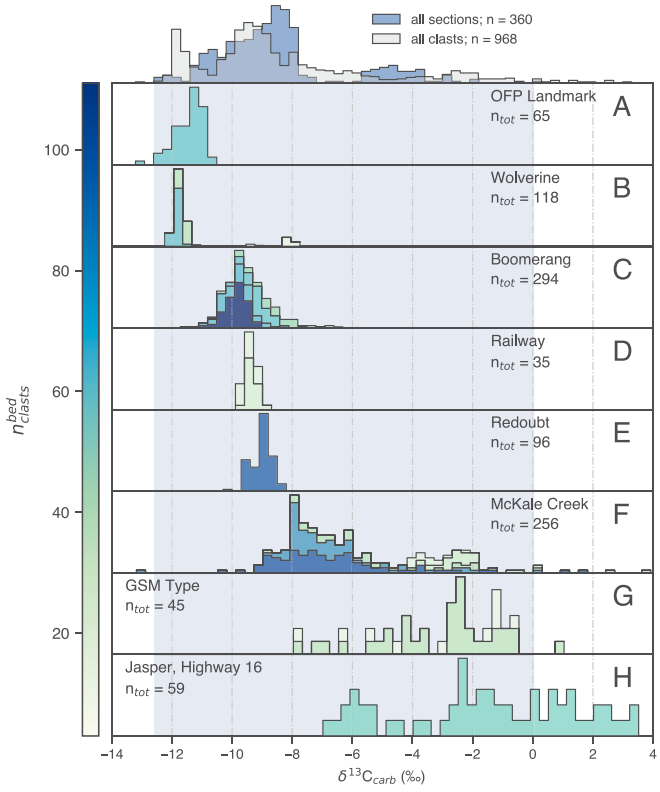

Fig. 7. Stacked histograms of $\delta^{13}C_{carb}$ values from carbonate clasts from breccia deposits of the Old Fort Point Formation (A-C, E-H), and the underlying Corral Creek Formation (D). Histograms are coloured by individual breccia bed horizon and grouped by locality. Sample size of clast populations from *individual* breccia beds (n) is indicated by the colour bar, and a composite histogram is shown for all clasts above (panel A) (grey). Alongside this distribution is the distribution of $\delta^{13}C_{carb}$ values of stratigraphic section data from the Old Fort Point Formation in blue (Fig. 4). This full range is shown behind each locality as a blue bar. Total clast populations (n_{tot}) for each locality are shown. Carbonates with positive values ($\delta^{13}C_{carb} \sim 0$ to 4‰) are found in breccia deposits at Jasper - Highway 16, and McKale Creek that are not found in the underlying or overlying stratigraphy and are interpreted to be sourced from either eroded or unsampled localities in the basin.

mineralogy of calcite. Early-diagenetic aragonite fans of this morphology have been described previously associated with the Shuram-bearing Ediacaran Johnnie Formation and have been interpreted to be shallow seafloor precipitates growing rapidly (potentially syn-depositionally within primary sediment) near the sediment–water interface (e.g. Pruss et al., 2008; Bergmann et al., 2013). Further, fans from the Johnnie Formation have $\delta^{13}C_{carb}$ values that are highly negative (~ –9 to –11‰). Similarly, the $\delta^{13}C_{carb}$ values exhibited by the aragonite fans of the Whitehorn Mountain Member range from ~ –9.5 to –10.5‰ (Figs. 6B, S2) suggesting that negative $\delta^{13}C$ values were perhaps being acquired in close proximity to seawater syn-depositionally. Though not preserved directly in the OFP stratigraphy, the presence of this material in several clasts of the WMM suggests that this process was occurring proximally to the source material of OFP carbonates. This is consistent with results of isotope conglomerate tests, and again makes burial dolomitization in association with organic matter remineralization or other diagenetic process an unlikely driver for the entire magnitude in $\delta^{13}C_{carb}$ values expressed in the OFP.

5.2. Early-marine diagenesis

Unlike the record of pelagic carbonates, carbonate platforms (such as those preserved in the Neoproterozoic) are subject to a myriad of local processes that can distort or even create spurious signals in the geochemical record. For example, carbonate sediments in the subsurface of the Great Bahama Bank have considerable variability in $\delta^{13}C_{carb}$ (~5‰) and do not have the same $\delta^{13}C_{carb}$ values or trends that are observed in coincident deep water sediment cores (Swart and Eberli, 2005; Swart, 2008; Higgins et al., 2018; Geyman and Maloof, 2021). Studies (e.g. Banner and Hanson, 1990; Higgins et al., 2018; Ahm et al., 2018) have shown that a multi-proxy approach using trace and major elemental abundances and isotopic measurements can aid in distinguishing between sediment-buffered diagenesis (reflecting the primary sediment) and fluid-buffered diagenesis (reflecting the composition of the diagenetic fluid). As the partition coefficients for elements such as Sr, Mn, and U into a carbonate lattice are vastly different between aragonite and calcite, these elements have great utility in the interpretations of diagenesis (e.g. Brand and Veizer, 1980). For example, Uranium has a notably higher partition coefficient in aragonite than calcite, therefore aragonite will have a higher U/Ca ratio than calcite precipitating out of the same seawater (e.g. Kitano and Oomori, 1971).

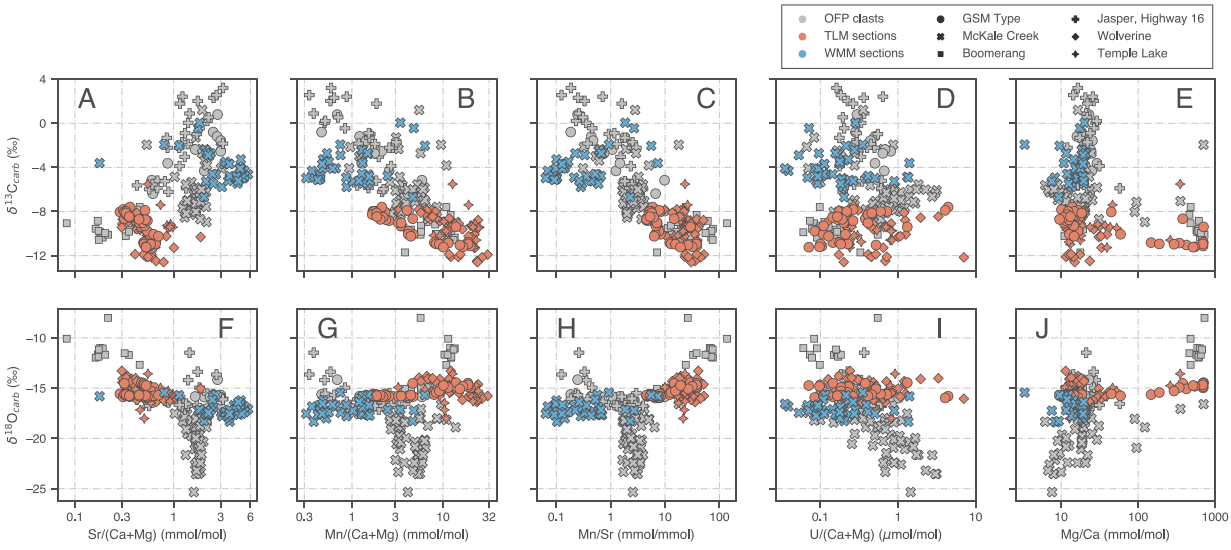

Fig. 8. Crossplots of elemental ratios (X/(Ca + Mg) except for Mg which is presented as Mg/Ca) vs $\delta^{13}C_{carb}$. All x-axes are logarithmic (mmol/mol or μmol/mol). Data are coloured by OFP member (WMM or TLM), vs clast populations (grey). Symbol type indicates locality.

Carbonates of the Temple Lake Member have Sr/(Ca + Mg) ratios that are higher in samples with more negative $\delta^{13}C_{carb}$ (Fig. 8A) which, in stratigraphic context, represents a decrease in Sr/(Ca + Mg) with stratigraphic height (Fig. 5). This trend in Sr/(Ca + Mg) is consistent with early-marine diagenesis and in particular, the neomorphism of a metastable aragonitic precussor to low-magnesium calcite. As shown by Higgins et al. (2018) and Ahm et al. (2018), modern primary platformal aragonite from The Bahamas has an approximate Sr/(Ca + Mg) ratio of 10 to 12 mmol/mol (Fig. 9), much higher than that shown in the TLM (< 1 mmol/mol generally, closer to diagenetic low-magnesium calcite (LMC)), suggesting either that the TLM sediment was originally calcitic, or that the diagenetic environment was strongly fluid-buffered by a low Sr fluid. The TLM is also characterized by a generally decreasing Mn/(Ca + Mg) with both stratigraphic position, and increasing $\delta^{13}C_{carb}$ (Figs. 5, 8D). Platform aragonites in The Bahamas are found to have Mn/(Ca + Mg) values < 0.1 mmol/mol (Higgins et al., 2018). Values of Mn/(Ca + Mg) are much higher compared to Bahamian aragonites. As subsurface (e.g. meteoric) fluids have been shown to be enriched in Mn and depleted in Sr (Brand and Veizer, 1980), the overall high Mn/(Ca + Mg) and low Sr/(Ca + Mg) (high Mn/Sr ratio, Fig. 8C) composition of the TLM carbonates suggests that open-system fluid-buffered recrystallization is a plausible explanation for the observed trends in Mn/(Ca + Mg) and Sr/(Ca + Mg) in the TLM (Fig. 9).

The WMM shows opposite trends in Sr/(Ca + Mg) and Mn/(Ca + Mg) to the TLM. Here, samples from McKale Creek are comparatively elevated in Sr/(Ca + Mg) (Fig. 8A). Values here (up to ~6 mmol/mol) are more similar to Bahamian aragonites, strongly suggesting the presence of an aragonite precursor. As in the TLM, a negative correlation is observed between stratigraphic height and Sr/(Ca + Mg) in the WMM, this time occurring alongside an increase in Mn/(Ca + Mg) (Fig. 5), similarly suggesting neomorphism of aragonite to LMC. However, the presence of high Sr/(Ca + Mg), and much lower Mn/(Ca + Mg) ratios (90% of samples < 3 mmol/mol), suggests that any recrystallization process occurring here was predominantly sediment-buffered, better retaining the Sr/(Ca + Mg) values of the original aragonitic sediment.

Geochemistry of clast populations suggest that the TLM and the WMM represent two distinct geochemical end-members each with their own unique diagenetic environment. Clast populations from all localities show a positive correlation between $\delta^{13}C_{carb}$ and Sr/(Ca + Mg) and a negative trend between $\delta^{13}C_{carb}$ and Mn/(Ca + Mg) (Fig. 10C, D) much like the trend between sections of the TLM and the WMM. The exception

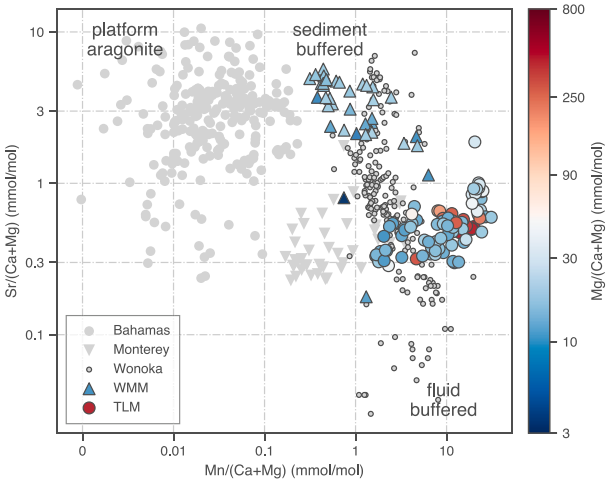

Fig. 9. Cross-plot of Mn/(Ca + Mg) vs Sr/(Ca + Mg) coloured by Mg/(Ca + Mg) ratio for the samples from stratigraphic sections of the TLM and WMM. Samples from shallow-water platform carbonates of the Bahamas (Higgins et al., 2018), authigenic dolomites of the Monterey Formation (Blättler et al., 2015), and Shuram-bearing carbonates of the Wonoka Formation of Australia (Husson et al., 2015) are shown in grey for comparison.

to the overall lower Mn/(Ca + Mg) ratios observed in the clasts (largely < 10 mmol/mol) are the dolomite clasts (Fig. 10D). These dolomites have the lowest $\delta^{13}C_{carb}$ values of the clast populations. Of all samples analyzed, 4% of stratigraphic section samples were found to be dolomitic, compared to 11% of breccia clast samples. Thus, diagenetic dolomite growth (intermittently influencing the geochemistry of TLM) seems to be preserved in breccia catchments of the WMM. The negative stratigraphic correlation with $\delta^{13}C_{carb}$, Sr/(Ca + Mg) and Mn/(Ca + Mg) is localized within the TLM and the broad-scale geochemical trend is better shown by low Sr/(Ca + Mg), high Mn/(Ca + Mg) TLM stratigraphy and the high Sr/(Ca + Mg) and low Mn/(Ca + Mg) WMM stratigraphy (as annotated on Fig. 10A). This trend in Sr/(Ca + Mg) and Mn/(Ca + Mg) over the WMM and TLM (Fig. 9) resembles trends observed in the Wonoka Formation of South Australia, a formation known to contain the Shuram CIE (Husson et al., 2015). Evidence from trace and major elements within clast populations of the OFP are in agreement with results of isotope conglomerate tests and $\delta^{13}C_{carb}$ values. Broad trends in these elements are consistent between in-place stratigraphy as well as within breccia clast populations further requiring and early origin of the $\delta^{13}C_{carb}$ signal in the OFP.

5.2.1. *Multivariate analyses*

To further explore the trends and possible processes controlling the entire geochemical dataset (both elemental ratios, X/(Ca + Mg), and isotopic values for all clasts and sections), principal component analysis (PCA) was used. PCA functions as a tool to reduce the dimensionality of a given dataset, and to linearly reproject the data onto orthogonal axes (principal components or eigenvectors) that contribute most to the total variance of the dataset. Results of PCA analysis on samples from the OFP are summarized in Fig. 11A-B. Analysis of covariance across all geochemical measurements suggests that the primary driver of variance is the influence of early diagenetic fluids. Principal Component 1 (PC1) (44.2% of the total explained variance) shows strong positive loadings for Li, Na, Mg, Al, Mn, Fe, Rb, U, $\delta^{18}O_{carb}$ and strong negative loadings for Sr and $\delta^{13}C_{carb}$ (Fig. 11A-B). As shown on the PCA biplot (Fig. 11A), loadings that have similar magnitude and direction are more correlated, and those that have opposing magnitudes and directions are anti-correlated. Thus, PC1 suggests a process where Sr/(Ca + Mg) and $\delta^{13}C_{carb}$ are anticorrelated with the rest of the dataset. This component is consistent with early-marine diagenetic restabilization of a metastable precursor (neomorphism of aragonite to calcite) in the presence of fluid with low $\delta^{13}C_{carb}$ values as described above, matching stratigraphic observations. Further, positive loadings of Li, Al, and Rb in PC1 suggest that these fluid interacted with siliciclatics before altering the OFP carbonates. Al/(Ca + Mg) is a commonly used indicator of detrital contamination (Dellinger et al., 2020; Wei et al., 2023). Most Al/(Ca + Mg) ratios in the OFP are largely < 1 mmol/mol, however some samples (particularly those with low Sr/(Ca + Mg)) have values up to 17 mmol/mol suggesting increased influence of detrital material, or leaching from clays during sample dissolution. If this excess Al is derived from increased detrital influence, reduction of oxide coatings on detrital minerals can provide another source of Mn to the sediments further explaining elevated Mn/(Ca + Mg) in the lower TLM (e.g. Burns and Baker, 1987).

Other trends in covariation of the data suggest a secondary and tertiary control by dolomitizing fluids. Loadings from PC2 and PC3 (15.87% and 13.16% of the total explained variance respectively) can be used. Scores on the PC2 axis in the presented PCA are dominantly controlled by positive loadings in $\delta^{18}O_{carb}$, $\delta^{13}C_{carb}$, Fe/(Ca + Mg) and Mg/Ca, and negative loadings in Mn/(Ca + Mg), Sr/(Ca + Mg), and U/(Ca + Mg). Further, negative loadings for Fe/(Ca + Mg) and Mg/Ca are observed in PC3. As dolomites are expected to have both higher Mg/Ca and $\delta^{18}O_{carb}$ (Brand and Veizer, 1981), and the distribution coefficient for Sr into dolomite is lower than that of calcite (Banner, 1995), these findings (particularly PC1) are consistent with a dolomitization

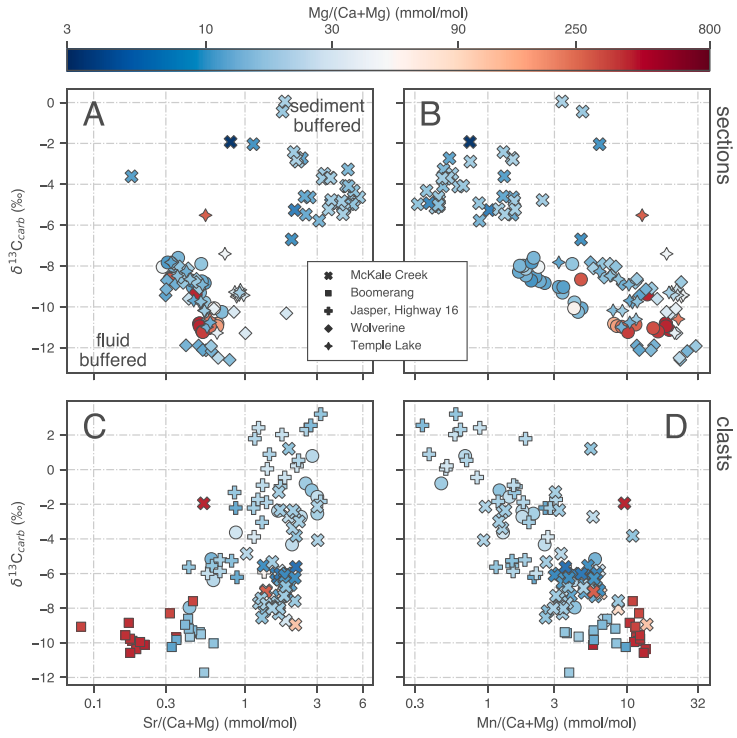

Fig. 10. Cross-plots of Sr/(Ca + Mg) and Mn/(Ca + Mg) vs $\delta^{13}C_{carb}$ for samples from stratigraphic sections (A, B), and breccia clasts (C, D) coloured by Mg/(Ca + Mg) ratio. Data are subset by locality and plotted on a logarithmic scale as in Fig. 8.

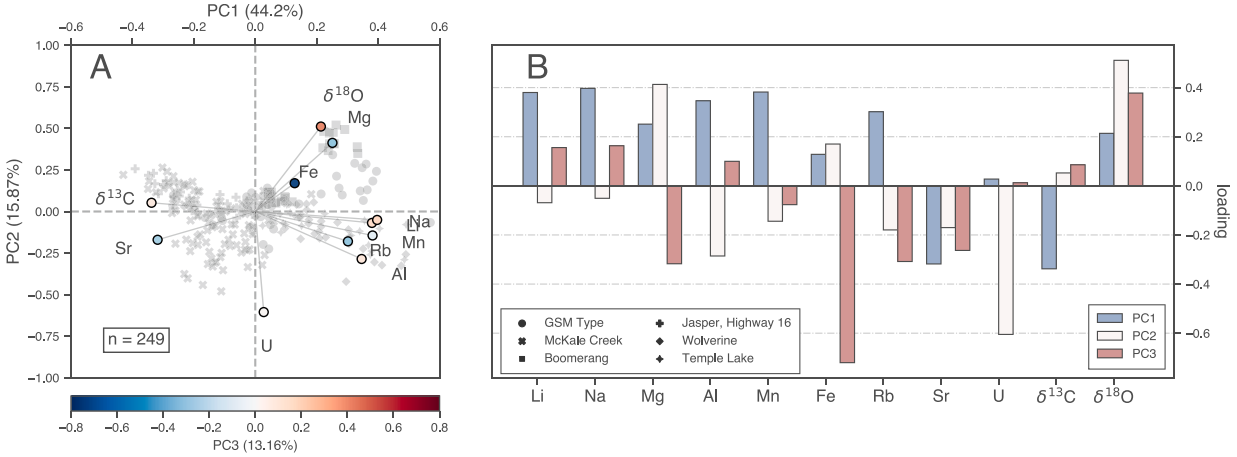

Fig. 11. (A) Resulting biplot from principal component analyses (PCA) of OFP multivariate dataset coloured by principal component (PC) 3. (B) PCA loading plots for PCA's 1–3 for each relevant component including all molar ratios, $\delta^{13}C_{carb}$ and $\delta^{18}O_{carb}$. All elements are molar ratios of X/(Ca + Mg).

pathway. Elevated values of Mg/Ca in TLM rhythmites range up to ~800 mmol/mol suggesting that dolomite is preserved in these units, though not consistently throughout the excursion interval. Moreover, dolomite is observed petrographically within samples from the basal TLM. Within this nadir $\delta^{13}C_{carb}$ interval, this dolomite is found to be blocky and inclusion rich, and seems to show visual evidence for burial recrystallization (obvious and strong twinning likely from recrystallization under pressure). The presence of dolomite within the lower TLM is evidence for fluid-buffered, early diagenesis as dolomite formation requires a large flux of fluid (i.e. seawater) derived Mg (Land, 1985). While values of Mg/Ca for both stratigraphic sections and clast populations are dominantly < 100 mmol/mol, many samples have values unlike stoichiometric dolomite (1000 mmol/mol) that range from 100 to ~800 mmol/mol (Fig. 8E, J). We interpret these elevated values of Mg/Ca to be physical admixtures of calcite and dolomite homogenized during bulk-rock drilling. In summary, the Temple Lake Member seems to have undergone early-marine diagenesis under fluid-buffered, partially dolomitizing conditions whereby primary aragonite is neomorphosed to either calcite or dolomite depending on shifts in the diagenetic fluid composition over time. The overlying WMM underwent diagenesis under more sediment-buffered conditions, preserving better the trace element geochemistry of an initially aragonitic precursor as indicative by the high Sr content (Figs. 8A, 10).

Based on the analyses and data presented, the $\delta^{13}C_{carb}$ composition of the Old Fort Point Formation is interpreted to be either the result of early-marine diagenesis, a record of basin water DIC distinct from the global average DIC pool, or a record of primary Ediacaran seawater DIC. Results of isotope conglomerate tests preclude late-stage (e.g. burial) diagenesis, yet it is difficult to ascertain exactly to what degree the $\delta^{13}C_{carb}$ signal has been altered by early diagenesis. Results demonstrate

that dolomitizing fluids and possible organic matter remineralization exert some level of control on carbonate containing nadir excursion values within the Temple Lake Member, yet Mg/Ca values within clast populations are dominantly low suggesting that there were few dolomites preserved in breccia catchments (and hence underlying stratigraphy). The discrete nature of dolomite horizons in the TLM coupled with generally low Mg/Ca values in clast populations suggests that dolomite formation did not widely alter the $\delta^{13}C_{carb}$ signal of the Temple Lake Member. $\delta^{13}C_{carb}$ values of OFP dolomites from the TLM are found to have broadly the same highly negative $\delta^{13}C_{carb}$ composition of concomitant calcites from stratigraphically adjacent, and correlative sections from other localities. Thus, despite studies demonstrating the ability of dolomitizing fluids and early marine diagenesis to alter records of $\delta^{13}C_{carb}$ (Blättler et al., 2015; Higgins et al., 2018; Ahm et al., 2018; Nelson et al., 2021), it seems that dolomitization is not leveraging $\delta^{13}C_{carb}$ values in the OFP. Trends in both Sr/(Ca + Mg) and Mn/(Ca + Mg) between clast populations and the in-place stratigraphy are characteristic of early diagenetic reactions. Geochemical analyses of clast populations coupled with chemostratigraphy from the overlying Whitehorn Mountain Member suggest that $\delta^{13}C_{carb}$ values of approximately –12‰ were acquired under relatively sediment-buffered conditions compared to those near –8‰ as seen in the TLM carbonates (Fig. 5), yet still more fluid-buffered than the carbonates of the WMM. Despite these findings, isotope conglomerate tests require the $\delta^{13}C_{carb}$ signal (diagenetic or not) to have been acquired early in the depositional history of the OFP.

5.3. Significance of $\delta^{13}C$ excursions in the Old Fort Point Formation

If the observed isotope excursion in the Old Fort Point Formation is a global phenomenon, several documented excursions from other continents could be potential correlative records of the same event. First, a CIE has been described from early in the Ediacaran known as the Weng'An Negative Carbon isotope Excursion (WANCE) from within the Doushantuo Formation in the Yangtze Gorges area of South China (Chen et al., 2022). The WANCE excursion is found to have a magnitude of ~ –10‰ and is constrained via U-Pb geochronology around 609 ± 5 Ma, similar in both magnitude and inferred age to the observed excursion in the OFP. If the excursion found within the TLM is indeed pre-Shuram and correlative to the WANCE, this would be the first observed occurrence of this excursion in western Canada. Also in the Yangtze Gorges area of South China, workers have identified a negative CIE, thought to be distinct from the Shuram, terminating at 550.1 ± 0.6 Ma (Yang et al., 2021). Though the age disparity between the proposed age of the OFP (607.8 ± 4.7 Ma) and the ~550 Ma excursion makes a correlation between the two events unlikely, the presence of this excursion highlights the prevalence of large magnitude isotopic variability within the Ediacaran. Finally, it is possible that given the sparse geochronology, the excursion interval within the OFP is correlated to the Shuram CIE, further arguing for the global nature of the event.

We have established through Mn/(Ca + Mg) and Sr/(Ca + Mg) ratios that it is likely that early diagenetic recrystallization from aragonite to calcite occurred within the OFP. Given these data and the carbonate-poor nature of the OFP, it is possible that local, early-marine diagenesis could be responsible for driving the OFP excursion towards more negative values and that the excursion is not age-diagnostic. As there are multiple highly negative excursion intervals throughout the Ediacaran, and diagenesis is often invoked to explain at least part of these, it implies that local diagenesis generating highly negative $\delta^{13}C_{carb}$ values are frequent over the Ediacaran. Diagenetic effects of meteoric fluids (e.g. Knauth and Kennedy, 2009), or interaction with low $\delta^{13}C_{carb}$ pore fluids (e.g. burial fluids, see Bristow and Kennedy, 2008; Derry, 2010) have been used to reconcile the mechanism for generating highly negative CIE values in the case of Shuram CIE. However such processes imply that, if the Shuram is synchronous, these diagenetic reactions are occurring synchronously within basins globally, a difficult phenomena to reconcile.

Early diagenesis can also be consistent with a global origin for the excursion observed in the OFP. The consistency in expression over a broad geographic area, low sample-to-sample variability, expression over a transgressive sequence, and our interpretation of $\delta^{13}C_{carb}$ values in the Old Fort Point Formation as representing either primary Ediacaran DIC or the product of early-marine diagenesis, suggests that the observed excursion could be equivalent to the Shuram CIE. An event that, regardless of its origin, represents a profound, seemingly synchronous (Rooney et al., 2020) shift in Ediacaran shallow-water chemistry related to either flux variations in the marine DIC pool, or globally-recorded local changes in platformal environments. Values of $\delta^{13}C_{carb}$ in the Old Fort Point Formation are similar to the Gametrail Formation of northwestern Canada (Macdonald et al., 2013; Moynihan et al., 2019; Busch et al., 2023) (see correlation in purple on Fig. 12B). Moreover, geochemical trends (e.g. Sr/(Ca + Mg) and Mn/(Ca + Mg)) within both OFP clast populations and stratigraphic sections are consistent with trends found in other Shuram-bearing localities such as the Wonoka Formation of Australia (Fig. 9). The presence of turbidites throughout Windermere deposition in the study region implies that the overall depositional setting is a relatively deep-water slope environment (Ross, 1991; Smith et al., 2014). Consistent differences in Shuram expression have been identified depending on the depositional environment, water depth, and hence, facies (Busch et al., 2022). Further, the most negative values of the Shuram excursion are expressed in slope environments (Busch et al., 2022). These differences in excursion expression with depth are consistent with the highly negative $\delta^{13}C_{carb}$ values of the Old Fort Point Formation and their inferred slope depositional environment.

Lithostratigraphically, the TLM shares a number of characteristics with the Shuram-bearing strata of western Laurentia. First, the Rainstorm Member of the Johnnie Formation in Death Valley, USA (Bergmann et al., 2011; Giles et al., 2023) is comprised of interbedded siltstones and limestones, and is known to contain calcite crystal fans thought to be pseudomorphs after aragonite much like those found in clasts of the WMM in the OFP (Fig. 3H - J). Additionally, like the Gametrail Formation of northern Canada, the OFP represents a transgressive sequence on the same continental margin (Ross, 1991), whereby a $\delta^{13}C_{carb}$ excursion occurs with concomitant base-level rise. Thus, geochemical shifts (such as $\delta^{13}C_{carb}$ excursions) along this margin should be broadly synchronous. Both the Johnnie and Gametrail Formations demonstrate pristine primary fabrics and facies including ooid shoals, stromatolitic horizons, and, as mentioned, seafloor crystal fans. All features that are absent from the in-place stratigraphy of the OFP. Carbonates of the Gametrail and Johnnie Formation reflect deposition in shallower, more platformal environments more likely to preserve primary carbonate fabrics, as well as shallower-water facies. Microbial fabrics in the OFP are largely absent with the exception of clasts in breccias of the WMM from OFP Landmark that display fine, crinkle-laminated fabrics reminiscent of cryptalgal microbialites, features quite common in younger sediments of nearby, Late Ediacaran platform carbonates of the Byng Formation in the Jasper region (e.g. Savage, 2004). Conversely, the inferred depositional mechanism of OFP carbonates is turbidite deposition along a deeper, slope environment. Deposition in such a way in a platform-distal environment prevents the preservation of many shallow-water facies and explains the lithological simplicity of preserved OFP carbonates.

Existing geochronology within the Windermere cannot rule out a Shuram occurrence within the OFP. While there is currently only one Re-Os age of 607.8 ± 4.7 Ma from the Geikie Siding Member of the OFP at GSM Type by Kendall et al. (2004), as highlighted in Fig. 12B and C, this age is inconsistent with presented geochemical data and with any of the current age estimates bracketing the Shuram (i.e. 574 ± 4.7 to 567.3 ± 3.0 Ma Rooney et al., 2020). If the ~608 Ma age is found to be reproducible (Fig. 12C), the presented data would lend support for a possible

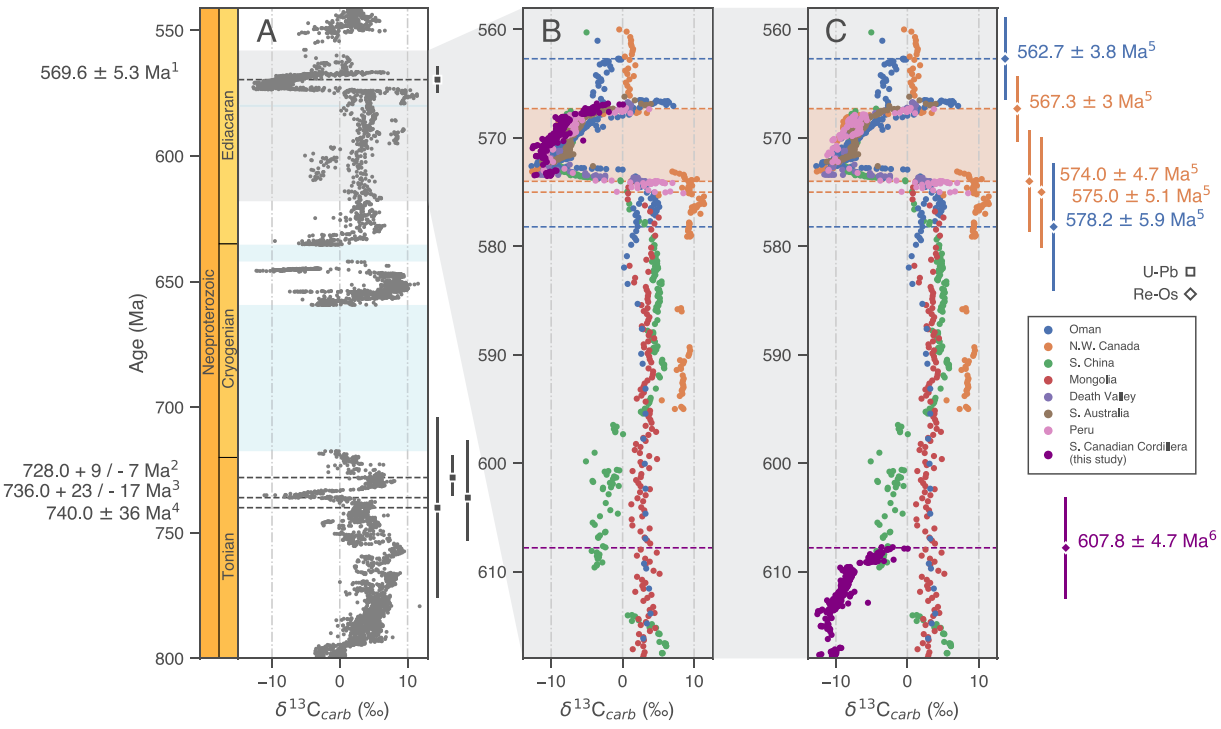

Fig. 12. Compilation of $\delta^{13}C_{carb}$ values (Ahm and Husson, 2022; Busch et al., 2022, this study), and geochronological constraints for the Neoproterozoic. (A) Neoproterozoic $\delta^{13}C_{carb}$ compilation with ages constraining deposition of the Windermere Supergroup in the southern Canadian Cordillera from Colpron et al. (2002)[1], Evenchick et al. (1984)[2], McDonough and Parrish (1991)[3], and Parrish and Scammell (1988)[4]. Glacial periods (stratigraphically, the Sturtian, Marinoan, and Gaskiers glaciations) are shown in blue. Two conceptual visual frameworks for OFP age-models are shown in (B) and (C) along with a composite $\delta^{13}C_{carb}$ curve for the Ediacaran with ages constraining the onset and recovery of the Shuram CIE (coloured by locality) from Rooney et al. (2020)[5] and the only known age produced from the Old Fort Point Formation to date (Kendall et al., 2004)[6]. A model rejecting the current Re-Os geochronology of the OFP deposition (607.8 Ma, Kendall et al., 2004) is shown in (B) with a simple age model generated by matching Shuram nadir values to those of the OFP. An alternative model accepting the 607.8 Ma age is shown in (C) with an age model generated based on the 607.8 Ma age in the overlying GSM. Note that in both cases we must emphasize the arbitrary nature of the generated age models due to a lack of robust geochronology in the Windermere.

correlation with the ~609 Ma WANCE, further implying that highly negative carbon isotope excursion events in the Ediacaran are not unique. If, conversely, the ~608 Ma age is proven too old (Fig. 12B) and and the depositional age of the OFP is closer to a ~578 to 563 Ma range as found to bracket the Shuram CIE (Rooney et al., 2020), it suggests that the excursion recorded by the carbonates of the TLM may be correlative to the Shuram CIE and, coupled with the geochemical data presented here, is the product of either Ediacaran seawater DIC or globally expressed local processes.

6. Conclusions

Across the southern Canadian Cordillera, the Old Fort Point Formation records a carbon isotope excursion with nadir values exceeding –12‰ preserved within a turbidite-generated carbonate sequence deposited in a deep-marine slope environment. Results of isotope conglomerate tests on carbonate clast populations require $\delta^{13}C_{carb}$ values of carbonates within the OFP to have been acquired near syn-depositionally, but pre-brecciation and before incision of WMM submarine canyons, ruling out a late-stage process such as burial diagenesis. Moreover, we show using trace and major elemental geochemistry that early-diagenetic marine fluids have likely influenced, in part, the preserved geochemical records. Rhythmic siltstones and carbonates of the TLM record the lowest $\delta^{13}C_{carb}$ values down to –12‰, while the overlying WMM deposition records the return to carbonate sedimentation and the expression of the excursion recovery from ~ –8 to 0‰. The consistency in the magnitude and vertical expression of this excursion across a broad geographic area matches observation from the Shuram-bearing Gametrail Formation of northwestern Canada (Busch et al., 2023). Both the OFP and the Gametrail Formation were deposited broadly during a transgression along the western margin of Laurentia. Coupling this with the unique geochemistry shared across both localities, we propose that the $\delta^{13}C_{carb}$ excursion preserved in both Formations are likely near synchronous. We therefore suggest that this excursion records the first noted expression of the Shuram carbon isotope excursion in the southern Canadian Cordillera, and that the current age constraints on OFP deposition (607.8 ± 4.7 Ma) are inconsistent with the presented geochemical evidence and that the sediments from which this age was generated must be re-analyzed.

CRediT authorship contribution statement

Connor S. van Wieren: Conceptualization, Investigation, Methodology, Formal Analysis, Visualization, Writing - original draft. **Jon M. Husson**: Conceptualization, Supervision, Resources, Writing - review & editing. **Blake Dyer**: Conceptualization, Supervision, Resources, Writing - review & editing.

Declaration of Competing Interest

The authors declare that they have no known competing financial interests or personal relationships that could have appeared to influence the work reported in this paper.

Data availability

All code and data required to reproduce the results of these analyses are accessible on Github (https://github.com/VanWieren/oldfortpoint_precambres).

Acknowledgements

We thank Tyler Hauk of the Alberta Geological Survey, and Dinu Pana of the Alberta Energy Regulator for field assistance and discussions that greatly benefitted this manuscript. Additionally, our interpretations and analyses benefitted significantly from discussions with Laurence Coogan, Paul Hoffman, Alan Rooney, Akshay Mehra, Brenhin Keller, Mark Smith, Anne-Sofie Ahm, and Stacey Edmonsond. We would like to thank Jerry Lei, Shannon Murtonen, and Morgan Weatherbie for assistance in the field. We would also like to thank Jody Spence for assistance in the lab at the University of Victoria. This research was funded by a Natural Sciences and Engineering Research Council of Canada (NSERC) Discovery Grants to J. Husson (RGPIN-2022–03230), and B. Dyer (RGPIN-2021–04082).

Appendix A. Supplementary material

Supplementary data associated with this article can be found, in the online version, at https://doi.org/10.1016/j.precamres.2024.107525.

References

Ahm, A.S., Husson, J., 2022. Local and Global Controls on Carbon Isotope Chemostratigraphy, 1 ed.,. Cambridge University Press. https://doi.org/10.1017/9781009028882.

Ahm, A.S.C., Bjerrum, C.J., Blättler, C.L., Swart, P.K., Higgins, J.A., 2018. Quantifying early marine diagenesis in shallow-water carbonate sediments. Geochim. Cosmochim. Acta 236, 140–159. https://doi.org/10.1016/j.gca.2018.02.042.

Aitken, J.D., 1969. Documentation of the sub-Cambrian unconformity, Rocky Mountains Main Ranges, Alberta. Can. J. Earth Sci. 6, 193–200. https://doi.org/10.1139/e69-018.

Banner, J.L., Hanson, G.N., 1990. Calculation of simultaneous isotopic and trace element variations during water-rock interaction with applications to carbonate diagenesis. Geochim. Cosmochim. Acta 54, 3123–3137. https://doi.org/10.1016/0016-7037(90)90128-8.

Banner, Jay.L., 1995. Application of the trace element and isotope geochemistry of strontium to studies of carbonate diagenesis. Sedimentology 42, 805–824. https://doi.org/10.1111/j.1365-3091.1995.tb00410.x.

Bergmann, K.D., Grotzinger, J.P., Fischer, W.W., 2013. Biological influences on seafloor carbonate precipitation. PALAIOS 28, 99–115. https://doi.org/10.2110/palo.2012.p12-088r.

Bergmann, K.D., Zentmyer, R.A., Fischer, W.W., 2011. The stratigraphic expression of a large negative carbon isotope excursion from the Ediacaran Johnnie Formation, Death Valley. Precambr. Res. 188, 45–56. https://doi.org/10.1016/j.precamres.2011.03.014.

Bjerrum, C.J., Canfield, D.E., 2011. Towards a quantitative understanding of the late Neoproterozoic carbon cycle. Proceedings of the National Academy of Sciences 108, 5542–5547. doi:10.1073/pnas.1101755108.

Blättler, C.L., Miller, N.R., Higgins, J.A., 2015. Mg and Ca isotope signatures of authigenic dolomite in siliceous deep-sea sediments. Earth Planet. Sci. Lett. 419, 32–42. https://doi.org/10.1016/j.epsl.2015.03.006.

Boag, T.H., Busch, J.F., Gooley, J.T., Strauss, J.V., Sperling, E.A., 2024. Deep-water first occurrences of Ediacara biota prior to the Shuram carbon isotope excursion in the Wernecke Mountains, Yukon. Canada. Geobiology 22, e12597. https://doi.org/10.1111/gbi.12597.

Boag, T.H., Darroch, S.A.F., Laflamme, M., 2016. Ediacaran distributions in space and time: Testing assemblage concepts of earliest macroscopic body fossils. Paleobiology 42, 574–594. https://doi.org/10.1017/pab.2016.20.

Bragg, W.L., 1924. The structure of aragonite. Proceedings of the Royal Society of London. Series A, Containing Papers of a Mathematical and Physical Character 105, 16–39. doi:10.1098/rspa.1924.0002.

Brand, U., Veizer, J., 1980. Chemical diagenesis of a multicomponent carbonate system - 1: Trace elements. J. Sediment. Res. 50, 1219–1236. https://doi.org/10.1306/212F7BB7-2B24-11D7-8648000102C1865D.

Brand, U., Veizer, J., 1981. Chemical Diagenesis of a Multicomponent Carbonate System - 2: Stable Isotopes. SEPM Journal of Sedimentary Research 51. https://doi.org/10.1306/212F7DF6-2B24-11D7-8648000102C1865D.

Bristow, T.F., Kennedy, M.J., 2008. Carbon isotope excursions and the oxidant budget of the Ediacaran atmosphere and ocean. Geology 36, 863. https://doi.org/10.1130/G24968A.1.

Burns, S.J., Baker, P.A., 1987. A geochemical study of dolomite in the Monterey Formation, California. J. Sediment. Res. 57, 128–139. https://doi.org/10.1306/212F8AC6-2B24-11D7-8648000102C1865D.

Burns, S.J., Matter, A., 1993. Carbon isotopic record of the Latest Proterozoic from Oman. Eclogae Geol. Helv. 86, 595–607.

Busch, J.F., Boag, T.H., Sperling, E.A., Rooney, A.D., Feng, X., Moynihan, D.P., Strauss, J. V., 2023. Integrated Litho-, Chemo- and Sequence Stratigraphy of the Ediacaran Gametrail Formation Across a Shelf-Slope Transect in the Wernecke Mountains, Yukon. Canada. American Journal of Science 323, 4. https://doi.org/10.2475/001c.74874.

Busch, J.F., Hodgin, E.B., Ahm, A.S.C., Husson, J.M., Macdonald, F.A., Bergmann, K.D., Higgins, J.A., Strauss, J.V., 2022. Global and local drivers of the Ediacaran Shuram carbon isotope excursion. Earth Planet. Sci. Lett. 579, 117368. https://doi.org/10.1016/j.epsl.2022.117368.

Carey, J.A., Simony, P.S., 1985. Stratigraphy, sedimentology, and structure of late Proterozoic Miette Group, Cushing Creek Area, B.C. Bull. Can. Pet. Geol. 33, 184–203. https://doi.org/10.35767/gscpgbull.33.2.184.

Charlesworth, H.A.K., Weiner, J.L., Akehurst, A.J., Bielenstein, H.U., Evans, C.R., Griffiths, R.E., Remington, D.B., Stauffer, M.R., Steiner, J., 1967. Precambrian Geology of the Jasper Region. Precambrian Geology of the Jasper Region. Research Council of Alberta Bulletin, p. 23.

Chen, B., Hu, C., Mills, B.J., He, T., Andersen, M.B., Chen, X., Liu, P., Lu, M., Newton, R. J., Poulton, S.W., Shields, G.A., Zhu, M., 2022. A short-lived oxidation event during the early Ediacaran and delayed oxygenation of the Proterozoic ocean. Earth Planet. Sci. Lett. 577, 117274. https://doi.org/10.1016/j.epsl.2021.117274.

Chew, D., Kirkland, C., Schaltegger, U., Goodhue, R., 2007. Neoproterozoic glaciation in the Proto-Andes: Tectonic implications and global correlation. Geology 35, 1095. https://doi.org/10.1130/G23768A.1.

Colpron, M., Logan, J.M., Mortensen, J.K., 2002. U-Pb zircon age constraint for late Neoproterozoic rifting and initiation of the lower Paleozoic passive margin of western Laurentia. Can. J. Earth Sci. 39, 133–143. https://doi.org/10.1139/e01-069.

Condon, D., Zhu, M., Bowring, S., Wang, W., Yang, A., Jin, Y., 2005. U-Pb Ages from the Neoproterozoic Doushantuo Formation, China. Science 308, 95–98. https://doi.org/10.1126/science.1107765.

Dellinger, M., Hardisty, D.S., Planavsky, N.J., Gill, B.C., Kalderon-Asael, B., Asael, D., Croissant, T., Swart, P.K., West, A.J., 2020. The effects of diagenesis on lithium isotope ratios of shallow marine carbonates. Am. J. Sci. 320, 150–184. https://doi.org/10.2475/02.2020.03.

Derry, L.A., 2010. A burial diagenesis origin for the Ediacaran Shuram-Wonoka carbon isotope anomaly. Earth Planet. Sci. Lett. 294, 152–162. https://doi.org/10.1016/j.epsl.2010.03.022.

Evenchick, C.A., Parrish, R.R., Gabrielse, H., 1984. Precambrian gneiss and late Proterozoic sedimentation in north-central British Columbia. Geology 12, 233–237. https://doi.org/10.1130/0091-7613(1984)12<233:PGALPS>2.0.CO;2.

Fike, D.A., Grotzinger, J.P., Pratt, L.M., Summons, R.E., 2006. Oxidation of the Ediacaran Ocean. Nature 444, 744–747. https://doi.org/10.1038/nature05345.

Fritz, W.H., Mountjoy, E.W., 1975. Lower and Early Middle Cambrian Formations near Mount Robson, British Columbia and Alberta. Can. J. Earth Sci. 12, 119–131. https://doi.org/10.1139/e75-013.

Geyman, E.C., Maloof, A.C., 2021. Facies control on carbonate δ13C on the Great Bahama Bank. Geology 49, 1049–1054. https://doi.org/10.1130/G48862.1.

Gibb, S., Pemberton, S.G., Chatterton, B.D.E., 2017. Arthropod Trace Fossils of the Upper Lower Cambrian Gog Group, Southern Rocky Mountains of Canada. Ichnos 24, 91–123. https://doi.org/10.1080/10420940.2016.1216845.

Giles, S.M., Christie-Blick, N., Lankford-Bravo, D.F., 2023. A subaerial origin for the mid-Ediacaran Johnnie valleys, California and Nevada: Implications for a diachronous onset of the Shuram excursion. Precambr. Res. 397, 107187. https://doi.org/10.1016/j.precamres.2023.107187.

Grotzinger, J.P., Fike, D.A., Fischer, W.W., 2011. Enigmatic origin of the largest-known carbon isotope excursion in Earth's history. Nat. Geosci. 4, 285–292. https://doi.org/10.1038/ngeo1138.

Halverson, G.P., Hoffman, P.F., Schrag, D.P., Maloof, A.C., Rice, A.H.N., 2005. Toward a Neoproterozoic composite carbon-isotope record. GSA Bulletin 117, 1181–1207. https://doi.org/10.1130/B25630.1.

Higgins, J.A., Blättler, C.L., Lundstrom, E.A., Santiago-Ramos, D.P., Akhtar, A.A., Crüger Ahm, A.S., Bialik, O., Holmden, C., Bradbury, H., Murray, S.T., Swart, P.K., 2018. Mineralogy, early marine diagenesis, and the chemistry of shallow-water carbonate sediments. Geochim. Cosmochim. Acta 220, 512–534. https://doi.org/10.1016/j.gca.2017.09.046.

Hoffman, P.F., Kaufman, A.J., Halverson, G.P., Schrag, D.P., 1998. A Neoproterozoic Snowball Earth. Science 281, 1342–1346. https://doi.org/10.1126/science.281.5381.1342.

Hoffmann, K.H., Condon, D., Bowring, S., Crowley, J., 2004. U-Pb zircon date from the Neoproterozoic Ghaub Formation, Namibia: Constraints on Marinoan glaciation. Geology 32, 817–820. https://doi.org/10.1130/G20519.1.

Hofmann, H.J., Mountjoy, E.W., 2001. Namacalathus-Cloudina assemblage in Neoproterozoic Miette Group (Byng Formation), British Columbia: Canada's oldest shelly fossils. Geology 29, 1091–1094. https://doi.org/10.1130/0091-7613(2001)029<1091:NCAINM>2.0.CO;2.

Husson, J.M., Higgins, J.A., Maloof, A.C., Schoene, B., 2015. Ca and Mg isotope constraints on the origin of Earth's deepest δ13C excursion. Geochim. Cosmochim. Acta 160, 243–266. https://doi.org/10.1016/j.gca.2015.03.012.

Husson, J.M., Maloof, A.C., Schoene, B., 2012. A syn-depositional age for Earth's deepest δ13C excursion required by isotope conglomerate tests. Terra Nova 24, 318–325. https://doi.org/10.1111/j.1365-3121.2012.01067.x.

Husson, J.M., Maloof, A.C., Schoene, B., Chen, C.Y., Higgins, J.A., 2015. Stratigraphic expression of Earth's deepest δ13C excursion in the Wonoka Formation of South Australia. Am. J. Sci. 315, 1–45. https://doi.org/10.2475/01.2015.01.

Jiang, G., Kaufman, A.J., Christie-Blick, N., Zhang, S., Wu, H., 2007. Carbon isotope variability across the Ediacaran Yangtze platform in South China: Implications for a large surface-to-deep ocean δ13C gradient. Earth Planet. Sci. Lett. 261, 303–320. https://doi.org/10.1016/j.epsl.2007.07.009.

Kendall, B.S., Creaser, R.A., Ross, G.M., Selby, D., 2004. Constraints on the timing of Marinoan "Snowball Earth" glaciation by 187Re–187Os dating of a Neoproterozoic, post-glacial black shale in Western Canada. Earth Planet. Sci. Lett. 222, 729–740. https://doi.org/10.1016/j.epsl.2004.04.004.

Kitano, Y., Oomori, T., 1971. The coprecipitation of uranium with calcium carbonate. J. Oceanogr. Soc. Jpn. 27, 34–42. https://doi.org/10.1007/BF02109313.

Knauth, L.P., Kennedy, M.J., 2009. The late Precambrian greening of the Earth. Nature 460, 728–732. https://doi.org/10.1038/nature08213.

Knoll, A., Walter, M., Narbonne, G., Christie-Blick, N., 2006. The Ediacaran Period: A new addition to the geologic time scale. Lethaia 39, 13–30. https://doi.org/10.1080/00241160500409223.

Kump, L.R., Arthur, M.A., 1999. Interpreting carbon-isotope excursions: Carbonates and organic matter. Chem. Geol. 161, 181–198. https://doi.org/10.1016/S0009-2541(99)00086-8.

Land, L.S., 1985. The Origin of Massive Dolomite. J. Geol. Educ. 33, 112–125. https://doi.org/10.5408/0022-1368-33.2.112.

Lanni, J.N., 2017. Old Fort Point Formation: Neoproterozoic Negative d13C Excursion Recorded in a Deep-Water Carbonate Succession. University of California Riverside, MSc Thesis.

Li, C., Hardisty, D.S., Luo, G., Huang, J., Algeo, T.J., Cheng, M., Shi, W., An, Z., Tong, J., Xie, S., Jiao, N., Lyons, T.W., 2017. Uncovering the spatial heterogeneity of Ediacaran carbon cycling. Geobiology 15, 211–224. https://doi.org/10.1111/gbi.12222.

Linnemann, U., Ovtcharova, M., Schaltegger, U., Gärtner, A., Hautmann, M., Geyer, G., Vickers-Rich, P., Rich, T., Plessen, B., Hofmann, M., Zieger, J., Krause, R., Kriesfeld, L., Smith, J., 2019. New high-resolution age data from the Ediacaran-Cambrian boundary indicate rapid, ecologically driven onset of the Cambrian explosion. Terra Nova 31, 49–58. https://doi.org/10.1111/ter.12368.

Macdonald, F.A., Strauss, J.V., Sperling, E.A., Halverson, G.P., Narbonne, G.M., Johnston, D.T., Kunzmann, M., Schrag, D.P., Higgins, J.A., 2013. The stratigraphic relationship between the Shuram carbon isotope excursion, the oxygenation of Neoproterozoic oceans, and the first appearance of the Ediacara biota and bilaterian trace fossils in northwestern Canada. Chem. Geol. 362, 250–272. https://doi.org/10.1016/j.chemgeo.2013.05.032.

Martin, M.W., Grazhdankin, D.V., Bowring, S.A., Evans, D.A.D., Fedonkin, M.A., Kirschvink, J.L., 2000. Age of Neoproterozoic Bilatarian Body and Trace Fossils, White Sea, Russia: Implications for Metazoan Evolution. Science 288, 841–845. https://doi.org/10.1126/science.288.5467.841.

McDonough, M.R., Parrish, R.R., 1991. Proterozoic gneisses of the Malton Complex, near Valemount, British Columbia: U-Pb ages and Nd isotopic signatures. Can. J. Earth Sci. 28, 1202–1216. https://doi.org/10.1139/e91-108.

McMechan, M., Waldron, J., 2015. The Neoproterozoic succession of the central Rocky Mountains, Canada. Bull. Can. Pet. Geol. 63, 243–273. https://doi.org/10.2113/gscpgbull.63.3.243.

Moynihan, D.P., Strauss, J.V., Nelson, L.L., Padget, C.D., 2019. Upper Windermere Supergroup and the transition from rifting to continent-margin sedimentation, Nadaleen River area, northern Canadian Cordillera. GSA Bulletin 131, 1673–1701. https://doi.org/10.1130/B32039.1.

Narbonne, G.M., Gehling, J.G., 2003. Life after snowball: The oldest complex Ediacaran fossils. Geology 31, 27. https://doi.org/10.1130/0091-7613(2003)031<0027:LASTOC>2.0.CO;2.

Nelson, L.L., Ahm, A.S.C., Macdonald, F.A., Higgins, J.A., Smith, E.F., 2021. Fingerprinting local controls on the Neoproterozoic carbon cycle with the isotopic record of Cryogenian carbonates in the Panamint Range. California. Earth and Planetary Science Letters 566, 116956. https://doi.org/10.1016/j.epsl.2021.116956.

Ostrander, C.M., Bjerrum, C.J., Ahm, A.S.C., Stenger, S.R., Bergmann, K.D., El-Ghali, M. A.K., Harthi, A.R., Aisri, Z., Nielsen, S.G., 2023. Widespread seafloor anoxia during generation of the Ediacaran Shuram carbon isotope excursion. Geobiology 21, 556–570. https://doi.org/10.1111/gbi.12557.

Parrish, R., Scammell, R., 1988. The age of the mount copeland syenite gneiss and its metamorphic zircons, Monashee Complex, southeastern British Columbia. Geologic Survey of Canada Paper 88, 21–28. https://doi.org/10.4095/126594.

Paul, D., Skrzypek, G., Fórizs, I., 2007. Normalization of measured stable isotopic compositions to isotope reference scales – a review. Rapid Commun. Mass Spectrom. 21, 3006–3014. https://doi.org/10.1002/rcm.3185.

Prave, A.R., Condon, D.J., Hoffmann, K.H., Tapster, S., Fallick, A.E., 2016. Duration and nature of the end-Cryogenian (Marinoan) glaciation. Geology 44, 631–634. https://doi.org/10.1130/G38089.1.

Pruss, S.B., Corsetti, F.A., Fischer, W.W., 2008. Seafloor-precipitated carbonate fans in the Neoproterozoic Rainstorm Member, Johnnie Formation, Death Valley Region, USA. Sed. Geol. 207, 34–40. https://doi.org/10.1016/j.sedgeo.2008.03.005.

Pu, J.P., Bowring, S.A., Ramezani, J., Myrow, P., Raub, T.D., Landing, E., Mills, A., Hodgin, E., Macdonald, F.A., 2016. Dodging snowballs: Geochronology of the Gaskiers glaciation and the first appearance of the Ediacaran biota. Geology 44, 955–958. https://doi.org/10.1130/G38284.1.

Rooney, A.D., Cantine, M.D., Bergmann, K.D., Gómez-Pérez, I., Baloushi, B.A., Boag, T. H., Busch, J.F., Sperling, E.A., Strauss, J.V., 2020. Calibrating the coevolution of Ediacaran life and environment. Proceedings of the National Academy of Sciences 117, 16824–16830. doi:10.1073/pnas.2002918117.

Rooney, A.D., Strauss, J.V., Brandon, A.D., Macdonald, F.A., 2015. A Cryogenian chronology: Two long-lasting synchronous Neoproterozoic glaciations. Geology 43, 459–462. https://doi.org/10.1130/G36511.1.

Ross, G., 1991. Tectonic setting of the Windermere Supergroup revisited. Geology 19, 1125. https://doi.org/10.1130/0091-7613(1991)019<1125:TSOTWS>2.3.CO;2.

Ross, G., Bloch, J., Krouse, H., 1995. Neoproterozoic strata of the southern Canadian Cordillera and the isotopic evolution of seawater sulfate. Precambr. Res. 73, 71–99. https://doi.org/10.1016/0301-9268(94)00072-Y.

Rothman, D.H., Hayes, J.M., Summons, R.E., 2003. Dynamics of the Neoproterozoic carbon cycle. Proceedings of the National Academy of Sciences 100, 8124–8129. doi:10.1073/pnas.0832439100.

Sahoo, S.K., Planavsky, N.J., Jiang, G., Kendall, B., Owens, J.D., Wang, X., Shi, X., Anbar, A.D., Lyons, T.W., 2016. Oceanic oxygenation events in the anoxic Ediacaran ocean. Geobiology 14, 457–468. https://doi.org/10.1111/gbi.12182.

Savage, D.A., 2004. Terminal proterozoic stromatolite reefs with shelly fossils, Salient Platform, British Columbia. Unpublished MSc Thesis.

Smith, M., Arnott, R., Ross, G., 2014. The Old Fort Point Formation: Redefinition and formal subdivision of a distinctive stratigraphic marker in the Neoproterozoic Windermere Supergroup, southern Canadian Cordillera. Bull. Can. Pet. Geol. 62, 1–13. https://doi.org/10.2113/gscpgbull.62.1.1.

Smith, M., Arnott, R., Ross, G., 2014. Physical and geochemical controls on sedimentation along an ancient continental margin: The deep-marine Old Fort Point Formation (Ediacaran), southern Canadian Cordillera. Bull. Can. Pet. Geol. 62, 14–36. https://doi.org/10.2113/gscpgbull.62.1.14.

Smith, M.D., 2009. Stratigraphic and geochemical evolution of the Old Fort Point Formation, southern Canadian Cordillera: the deep-marine perspective of Ediacaran post-glacial environmental change. PhD Thesis.

Swart, P.K., 2008. Global synchronous changes in the carbon isotopic composition of carbonate sediments unrelated to changes in the global carbon cycle. Proceedings of the National Academy of Sciences 105, 13741–13745. doi:10.1073/pnas.0802841105.

Swart, P.K., Eberli, G., 2005. The nature of the δ13C of periplatform sediments: Implications for stratigraphy and the global carbon cycle. Sed. Geol. 175, 115–129. https://doi.org/10.1016/j.sedgeo.2004.12.029.

Verdel, C., Wernicke, B.P., Bowring, S.A., 2011. The Shuram and subsequent Ediacaran carbon isotope excursions from southwest Laurentia, and implications for environmental stability during the metazoan radiation. GSA Bulletin 123, 1539–1559. https://doi.org/10.1130/B30369.1.

Wei, G.Y., Zhang, F., Yin, Y.S., Lin, Y.B., Pogge von Strandmann, P.A.E., Cao, M., Li, N., Xiong, G., Chen, X., Fan, C., Xu, C., Tan, F., Zhang, X., Yang, H., Ling, H.F., Shen, S. Z., 2023. A 13 million-year record of Li isotope compositions in island carbonates: Constraints on bulk inorganic carbonate as a global seawater Li isotope archive. Geochim. Cosmochim. Acta 344, 59–72. https://doi.org/10.1016/j.gca.2023.01.013.

Wood, R., Curtis, A., 2015. Extensive metazoan reefs from the Ediacaran Nama Group, Namibia: The rise of benthic suspension feeding. Geobiology 13, 112–122. https://doi.org/10.1111/gbi.12122.

Xiao, S., Laflamme, M., 2009. On the eve of animal radiation: Phylogeny, ecology and evolution of the Ediacara biota. Trends in Ecology & Evolution 24, 31–40. https://doi.org/10.1016/j.tree.2008.07.015.

Xiao, S.H., Narbonne, G.M., 2020. Chapter 18 - The Ediacaran Period, in: Gradstein, F. M., Ogg, J.G., Schmitz, M.D., Ogg, G.M. (Eds.), Geologic Time Scale 2020. Elsevier, pp. 521–561. doi:10.1016/B978-0-12-824360-2.00018-8.

Yang, C., Rooney, A.D., Condon, D.J., Li, X.H., Grazhdankin, D.V., Bowyer, F.T., Hu, C., Macdonald, F.A., Zhu, M., 2021. The tempo of Ediacaran evolution. Sci. Adv. 7, eabi9643. https://doi.org/10.1126/sciadv.abi9643.